Natural oil seep systems in the Aegean Sea

Romain Jatiault, Pierre Henry, Lies Loncke, Mahrez Sadaoui, Dimitris Sakellariou

Marine and Petroleum Geology xxx (xxxx) 106754

Contents lists available at ScienceDirect

Marine and Petroleum Geology

journal homepage: www.elsevier.com/locate/marpetgeo

Natural oil seep systems in the Aegean Sea

Romain Jatiault [a, *], Pierre Henry [c], Lies Loncke [a], Mahrez Sadaoui [a], Dimitris Sakellariou [b]

[a] University of Perpignan Via Domitia, Centre de Formation et de Recherche sur les Environnements Méditerranéens (CEFREM), UMR 5110, 52 Avenue Paul Alduy, 66100, Perpignan, France
[b] HCMR, Hellenic Centre for Marine Research, Anavyssos, Greece
[c] Aix Marseille Univ, CNRS, IRD, INRAE, Coll France, CEREGE, Aix-en-Provence, France

ARTICLE INFO

Keywords:
Seeps
Fluids
Oil
Satellite
Mass transport deposits
Aegean
North anatolian fault

ABSTRACT

The analysis of satellite-based Synthetic Aperture Radar Sentinel-1 data reveals the presence of an oil seepage system composed of 33 recurrent oil seeps sites in the Aegean Sea. The temporal analysis of this system shows that most oil seeps are detected during the summer period, probably due to better detection conditions during this period. The estimations of expulsion frequency computed using the summer period show that the frequency is highly variable from one seep to another with occurrence rates that reach 40% for the most active sites. Oil seeps gather among two main provinces. First, in the Limnos and Saros pull-apart basins where oil seeps are aligned along the North Anatolian Fault (NAF), which suggest that oil seep locations are mostly driven by the fault network. In the Limnos basin, detected oil seeps also coincide with the location of a gravity-driven sedimentary destabilisation complex that developed under the influence of the Limnos pull-apart basin subsidence and the transtensive strain of the NAF. Finally, oil seeps detected in the proximity of the Skyros-Edremit region seems to follow a different control considering that oil seeps appear disconnected from the main fault in the area (Skyros-Edremit).

1. Introduction

Since the advent of satellite imagery, and in particular the radar system (synthetic aperture radar; McCandless and Jackson, 2003), the detection and recognition of offshore oil expulsion sites has been conducted in many sedimentary basins (Dong et al., 2022), whether carried out by academic research in order to better understand its implication on the marine environment (role in carbon balances; chemosynthetic and deep-sea communities distribution; Ondreas et al., 2005; Judd and Hovland, 2009; Jones et al., 2014), or by the petroleum industry in order to characterise offshore petroleum prospects (Meurer et al., 2023). Monitoring fluid emissions along major active faults from space provides a remote and regional vision of fluid escape situation that can further be compared with local geological settings or seismic activity (Geli et al., 2018; Henry et al., 2018; Sultan et al., 2022).

The recognition of these expulsion systems is performed through the interpretation of successive satellite images. The orientation of oil slicks is driven by surface winds and currents which can be highly variable over time, but the surfacing point of the oil droplets at the sea surface always occur among a restricted sized area (Macdonald et al., 1993; Crooke et al., 2015; Jatiault et al., 2018). Thus, mapping slicks on a stack of images produces divergent patterns easily recognisable from a central point. The identification of recurrent seepage slicks with spaceborne SAR (Synthetic Aperture Radar) provides a regional overview of oil seeping provinces that can be directly overlain on geological datasets allowing to better understand the geological settings involved in the expulsion process (Garcia-Pineda et al., 2010).

A consistent fraction of sedimentary basins has been investigated and recognised as associated with recurrent natural oil slicks (Dong et al., 2022). The provinces identified as naturally emitting the highest oil volumes are the Gulf of Mexico (MacDonald et al., 1993), the Caspian Sea (Zatyagalova et al., 2007) and the West African margin (Jatiault et al., 2017; Najoui et al., 2022). The oil potential being greater, passive margin has been extensively surveyed by the oil industry for oil seepages (Gulf of Mexico and Lower Congo Basin), conversely to active margins. However, several studies show that tectonics and structural context is a main controlling factor on fluid expulsion systems (Macgregor, 1993; Loncke and Mascle, 2004; Zitter et al., 2006). Among geological factors, faults zones are potential conduits for fluid migration and are known to influence the distribution of fluid emissions (cold seeps) at the seafloor in tectonically active settings (e.g. Sibuet et al., 1988; Henry et al., 1989; Jollivet et al., 1990; Bohrmann et al., 2002; Orange

* Corresponding author.
E-mail address: romain.jatiault@univ-perp.fr (R. Jatiault).

https://doi.org/10.1016/j.marpetgeo.2024.106754
Received 24 November 2023; Received in revised form 2 February 2024; Accepted 11 February 2024
0264-8172/

et al., 2002; Zitter et al., 2008; Barnes and Pondard, 2010; Suess, 2014; Le Pichon et al., 2016; Henry et al., 2018). Up to now, few active or passive transform margins are recorded as being associated with oil expulsion zones. Even if transform margins systems appear to be widely distributed around the world and to mediate vertical fluid flow (Mercier de Lépinay et al., 2016; Hensen et al., 2019), relatively few oil seeps have been reported in such strike-slip systems even if active gas emissions has been described into the water column especially in active transform settings (Dupre et al., 2015), (e.g. Allen et al., 1970; Ruffine et al., 2018). Strike-slip systems are subjected to high variability of stress regime over short-scale zones, especially along "in echelon" systems (e.g., Gulf of California; Stock and Hodges, 1989; Canet et al., 2010; Arango-Galván et al., 2015). Depending on the fault configuration, those systems can be associated with transpressive (generate thrust faults and pop-up areas), or transtensive (pull apart basin systems) components.

The discovery of natural oil seeps in the Aegean Sea (Dong et al., 2022), which is a back-arc basin bounded by the transform North Anatolian Fault, provides an opportunity to study the mechanisms of fluid expulsion in this geological environment. Observations of the North Anatolian Fault led to formulate hypotheses that require long term monitoring for their testing (Geli et al., 2018; Henry et al., 2018; Sultan et al., 2022). Natural oil seepages are considered as possible sources of disturbances to biogeochemical processes in the water column (e.g. Solomon et al., 2009; Camilli et al., 2010; Joye et al., 2011; Korber et al., 2014; Jatiault et al., 2021). For instance, oceanographic studies of the Aegean Sea basins have found anomalous oxygen consumption in Limnos Basin, with unclear causes (Zervakis et al., 2003). This margin system presents potentially varied tectonic regimes with alternating pure transform/strike-slip faults and transpressional and transtensional bends. These environments represent a unique opportunity to study the effect of stress regimes on fluid expulsion. The aim of this paper is to detail the oil seeps sites discoveries over the Aegean Sea and to provide a first vision of the geological contexts involved in the emplacement of these systems.

2. Geological context of the North Aegean Sea

2.1. Ocean conditions of the Aegean Sea

The North Aegean Sea is a semi-enclosed sea with hydrological exchanges with the Southern Aegean Sea taking place through the straits crossing the Cyclades area and is hydrologically connected with the Sea of Marmara through the Dardanelles Strait (Fig. 1a). From a bathymetric point of view, this sea is associated with strong variations in water depth and two main contexts are represented: shallow areas (0–200 m) associated with the continental shelf and deeper basins (700–1500 m) such as the Saros trough, the North Aegean trough and the Skyros-Edremit trough which are all associated with regional and crustal-rooted transform or strike-slip faults (Fig. 1b). The transition zones have steep slopes and are associated with the flanks of these regional faults.

The North Aegean water is subject to intrusions of low salinity Marmara and Black Sea surface water through the Dardanelle straight and of higher salinity Western Mediterranean Sea water from the South (Spondylidis et al., 2020). Due to important water depth variations between the shelf and the deep troughs (North Aegean, Saros, Skyros-Edremit), the water circulation is affected by strong vertical water transfers, notably upwellings related to prevailing northerly winds in summer (e.g., Androulidakis et al., 2017). This restricted and confined environment also generates multiple reflection loops and gyres (around Samosraki, Sporadhes, Athos and Skyros-Edremit gyres). Due to the site configuration, strong variations of the average current velocity were modelled (Estournel et al., 2021). The Dardanelle input only affects the upper water layer and appears stronger in summer forming eddies around Samosraki and Saros basin.

2.2. Tectono-stratigraphic framework

The Aegean Sea is a back-arc type basin developed above the northward subducting East Mediterranean lithosphere. The rate of SSW-ward stretching of the Aegean crust (roughly 2–3 cm yr^{-1} today) is higher than the rate of convergence between Africa and Eurasia (~5–6 mm. yr^{-1}) and results in an extensional regime (Reilinger et al., 2006; Taymaz et al., 2007; Jolivet et al., 2008; Le Pichon and Kreemer, 2010).

The tectonic history of the Aegean region since the Eocene has been driven by the southward retreat of the Hellenic subduction and the subsequent extension of the overriding crust perpendicular to the curved Hellenic arc. Later, the onset of the movement of the Anatolian plate towards West since Miocene, accommodated by the dextral North Anatolian Fault, modified the style of deformation of the Aegean Region. The propagation of the North Anatolian Fault Zone branches into the North Aegean Sea since Late Miocene or Pliocene and the associated dextral shearing led to the establishment of a transtensional regime and accel-

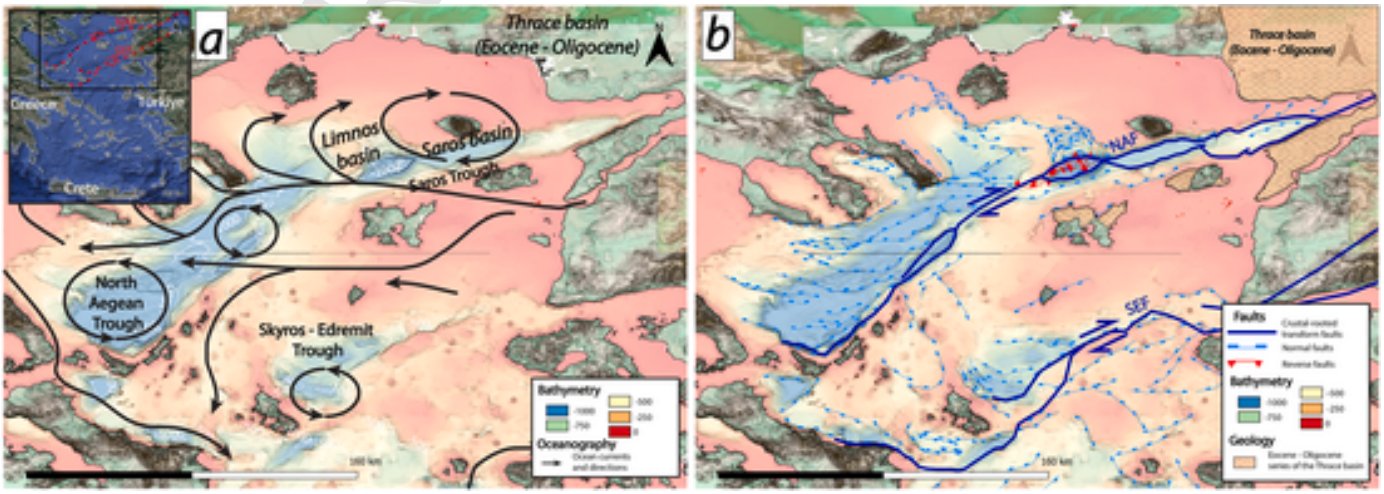

Fig. 1. a. Bathymetric map of the North Aegean Sea (EMODNET – see insert map in top left corner) overlain with the main reported currents across the area (Tzali et al., 2010; Spondylidis et al., 2020). The annotation on the map corresponds to the deeper basins among the North Aegean Sea. b. Bathymetric map overlain with the morpho-bathymetric interpretation of seafloor fault locations (compiled and modifier after Sakellariou et al., 2016; Jolivet et al., 2013; Brun et al., 2016; Erbil et al., 2021).

erated the SSW-ward stretching of the Aegean (Mascle and Martin, 1990; Jolivet et al., 2008; Armijo et al., 1999; Brun et al., 2016). Nowadays, the North Aegean Sea is crossed by two main fault systems which are (i) the North Anatolian Fault Zone (northern active branch) and (ii) the Skyros-Edremit Fault Zone (SEF) (southern branch of the North Anatolian Fault; Le Pichon et al., 2003; Şengör et al., 2005; Jolivet et al., 2008; Tsampouraki-Kraounaki and Sakellariou, 2018; Papanikolaou et al., 2019). Those bound a ~100 km wide deformation zone (Reilinger et al., 2006, Fig. 1). The tectonic stress regime of the basin progressively evolves from a dominantly transtensional strike-slip regime in the Eastern part towards a more extensional regime at the fault terminations in the west (Jolivet et al., 2008; Brun et al., 2016; Sakellariou and Tsampouraki-Kraounaki, 2019). This is evidenced from the horse tail systems at the termination of both NAF and SEF, visible in the North Aegean trough and Skyros-Edremit trough (Fig. 1b). The markers of the extensional strike-slip regime occur along the two major faults and are notably visible by the development of numerous pull apart basin systems (Saros Trough, North Aegean Trough and Skyros-Edremit Trough). The active subsidence of the Limnos basin is evidenced from the presence of several successive escarpments visible in the seafloor morphology, North of the basin (Fig. 1b). Some of these escarpments are associated with gravity-driven deformation, for example like the sliding mass affecting Pliocene and Quaternary series towards the Limnos basin (Tsampouraki-Kraounaki and Sakellariou, 2018). Manifestations of transpressive relays are also visible in the Limnos basin with the occurrence of a thrust belt along the Limnos basin edge which generates a topographic high pop-up anticline (Sakellariou et al., 2016). The tectonic stress regime is therefore complex along the NAF and associated with strong lateral modifications.

A series of synclinal and anticlinal folds located onshore north of the North Anatolian Fault (Ganos area) mainly involve Eocene-Oligocene sediments of the Southern Thrace Basin (Fig. 1b; Erbil et al., 2021). In contrast, the folds to the south of the fault also involve Miocene deposits, with identical styles and no significant unconformity (Armijo et al., 1999).

The SEF initiated 2–3 Ma years ago, originates East of the Sea of Marmara (Dokursun) and runs across Turkey until the Gulf of Edremit (Le Pichon et al., 2003; Şengör et al., 2005; Jolivet et al., 2008) and induce a dextral movement between the Anatolian plate and the North of the Aegean Sea. The SEF is also partly transtensive and associated with a typical horse tail system which triggers the formation of the Skyros-Edremit trough at its termination (similar to the NAF termination in the North Anatolian trough). The Upper Eocene-Oligocene shales of the Thrace basin (Siyako and Huvaz, 2007; Gürgey, 2009; 2015) are reported with a high total organic matter. In the onshore domain, the Paleogene/Eocene silici-clastic of the Thrace basin are high potential source rocks ().

3. Data and methods

3.1. Satellite imagery

The data used are radar images (Synthetic Aperture Radar; C-Band) from the Sentinel 1 A and Sentinel 1 B satellites, respectively launched the April 3rd, 2014, and April 25th, 2016. Sentinel-1 operates in four acquisition modes: Stripmap (SM), Interferometric Wide swath (IW), Extra-Wide swath (EW), and Wave (WV). Each mode can potentially produce different products: at level 0 - SAR (Synthetic Aperture Radar), at level 1 – SLC (Single Look Complex), at level 1 GRD (Ground Range Detected) and at level 2- OCN (Ocean). Data products are available in single polarization (VV or HH) for Wave mode and dual polarization (VV + VH or HH + HV) or single polarization (HH or VV) for SM, IW and EW modes. The analyzed Sentinel-1 data in this study were acquired in Interferometric Wide Swath (IW) mode, VV polarization and processed to Level 1 - Ground Range Detection (GRD). The pixels size of IW mode is 10*10 m and with a swath width of 250 km. The data were either collected through the Copernicus website (https://scihub.copernicus.eu/) and the DIAS (Data and Information Access Services) of Copernicus. These DIAS are cloud-based platforms allowing centralized access to data and information, as well as Copernicus processing tools. The images were processed using SNAP toolboxes following the processing chain: thermal noise removal; Calibration; noise level reduction Multilook; Ellipsoid-Correction-GG; Linear To dB conversion.

The study was carried out in two stages, firstly the whole of the North Aegean was analyzed on a relatively small time scale (Summer, 2019 and 2020; blue colour scale: Fig. 2), then a second phase of analysis of the full data stack was carried out on selected sites that showed recurrent patterns and were potentially associated with fluid expulsions (red colour scale: Fig. 2). The satellite data used in this study over the Aegean Sea, covers the full Sentinel-1 data stack between launch until March 2022. The revisit period over the Aegean is at least every 3–4 days, the coverage varies from 900 of up to 1600 images in this study (Fig. 2). A total of 4000 images were analyzed considering multiple satellite acquisition swath across the entire Aegean Sea. Satellite images were analyzed in the QGIS mapping software.

Seepage slicks detection is based on the analysis of radiometric anomalies associated with oil-covered areas and were manually delineated. Diverging structures on the stack of slick outlines highlights recurrent oil seeps due to current variability at the sea surface; their centre pinpoints the locations of active oil seeps (Garcia-Pineda et al., 2010). We draw visually the Oil Slick Origins (OSO, Garcia-Pineda et al., 2010; Korber et al., 2014) from the location of the proximal detectable edge of each oil slick. Delineated slicks were afterward confirmed using deep neural networks (Scardigli et al., 2023). Spatial attributes were computed for each slick, such as the date and name of the image, the type of occurrence, the confidence index, the surface area, and length. The confidence index displays the degree of discrimination of liquid hydrocarbons compared to the different look-alikes (bioturbations, algal blooms, pollution; Najoui et al., 2022). The Oil Slick Origin (OSO; Garcia-Pineda et al., 2010) is defined for the proximal detectable location of each slick from the centre recurrent seepage area. The OSO were determined for each slick or recurrent structure detected in the Saros basin. The hydrocarbon occurrence rate (in %) was calculated from the ratio between the number of identified hydrocarbon slicks and the satellite data coverage.

3.2. High resolution seismics

The seismic data presented here were acquired in 2015 by the Hellenic Centre for Marine Research with R/V Aegaeo, during the "YPOTHER/Aegean Explorations" project funded in the framework of Greece structural funding program. An airgun with 40in^3 air-chamber, triggered at 4 s rate, and a SIG streamer, Model 16.48.65, 65 m length with 48 hydrophones at 1 m spacing were used for the acquisition of the seismic profiles (Sakellariou et al., 2016).

4. Results and discussions

4.1. Oil seeps sites inventory in the Aegean Sea

The overlay of the successive oil slick events detected from the analysis of satellite data reveals typical and characteristic patterns of natural oil expulsion zones. The compilation slicks map shows divergent structures from different central points. The centre of those structures inform about the oil impact area on the sea surface (Fig. 3). A total of 3300 slicks were detected across the Aegean Sea based on the interpretation of the 2014–2022 Sentinel-1 SAR dataset, which corresponds to a data pile of 4000 images. A total of 34 active and recurrent oil seeps

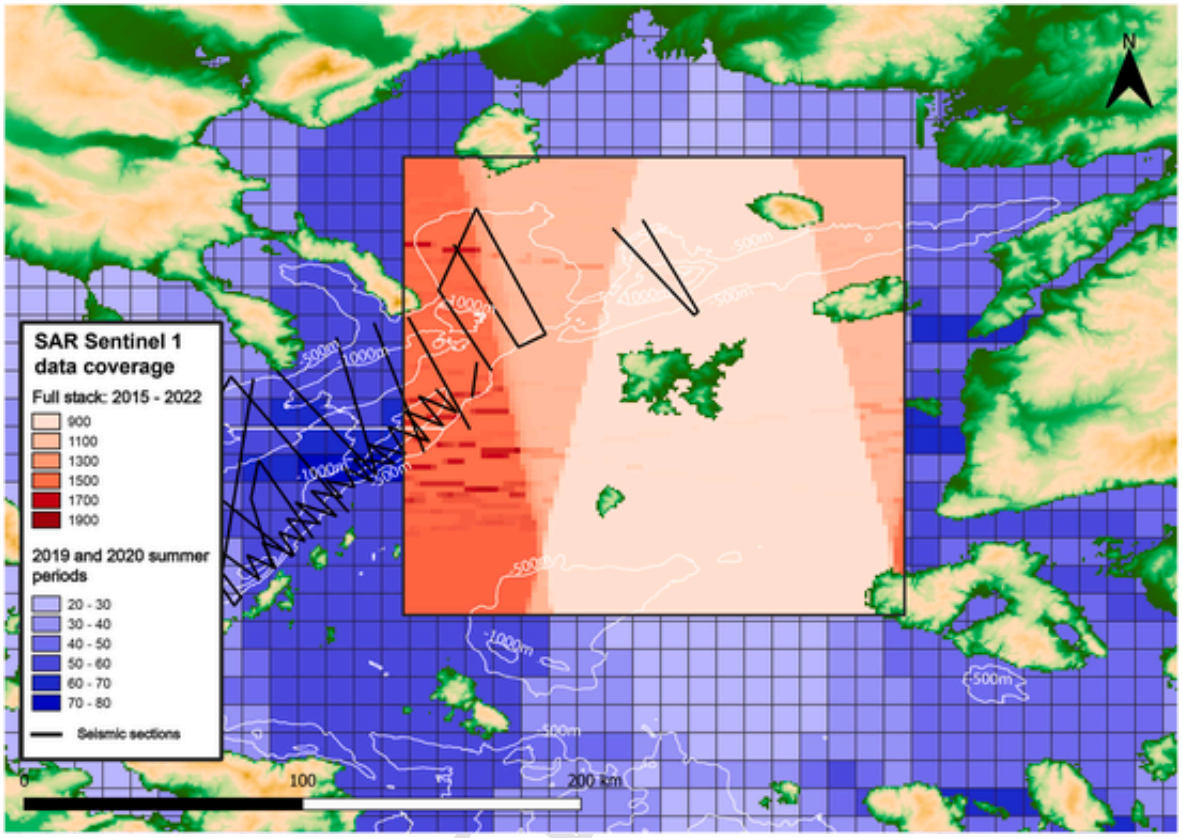

Fig. 2. SAR image density stack. The colour shows the amount of repetitive available SAR images. The blue scale displays the dataset of the first study performed over the entire Aegean Sea. The red scale displays the zoom in the North Aegean Sea where the amount of interpreted data is much higher. The location of available seismic lines is indicated in bold black lines.

sites are detected and clustered among 4 different provinces across the Aegean Sea (Fig. 3).

Regarding the geological context, the natural oil expulsion zones detected are located within two distinct areas. The first area is in the North along the North Anatolian Fault (NAF), associated with the "en echelon" pull apart basins forming the Saros Trough in the North. The second is the central part of the Aegean Sea, at Northern edge of the Skyros-Edremit trough (Fig. 3). Among these two regions, oil seeps are concentrated among 5 distinct areas, namely oil seeps cluster (Jatiault et al., 2018).

4.1.1. Temporal distribution

The temporal analysis of the distribution of the detected slicks on the Sentinel-1 image stack reveals some periods over the year during which the detection of oil slicks is significantly higher (Fig. 4). Detection pulses gathered among the summer period suggest a seasonal bias in the detection between autumn to spring (Fig. 4a). In particular, the number of detected slicks is much higher during June, July and August (Fig. 4b).

A consistent portion of Sentinel-1 images remained uninterpreted due to the large number of look-alikes such as biofilms visible during certain periods (mainly autumn and spring). The detection of oil is strongly conditioned by the meteorological conditions and by the wind speed at the origin of the formation of capillary waves which make it possible to discriminate between open water and water covered by oil (Franceschetti et al., 2002; McCandless and Jackson, 2003). The minimum detection speed is between 1.5 (Skrunes, 2014; Fingas and Brown, 2014; Jatiault et al., 2017) and 3 m.s^{-1} (Espedal and Wahl, 1999; Johannessen et al., 2000; Girard-Ardhuin et al., 2005, Brekke and Solberg, 2005), while the higher velocity seems to be dependent on the origin and thickness of the oil slicks (5 m s^{-1} for natural thin slicks; Bern et al., 1992; Espedal and Wahl, 1999; Garcia-Pineda et al., 2009; Jatiault et al., 2017; up to 10 m s^{-1} for thicker slicks; Fingas and Brown, 2014). The main wind direction in the North Aegean is towards the southwest (Soukissian and Sotiriou, 2022) and seems constant throughout the year (Vagenas et al., 2017). The average variability of wind within a year is estimated at 60% (Soukissian and Sotiriou, 2022). For the islands of Samosraki and Lemnos, which are close to areas with natural discharges, the average velocities are 8 m s^{-1} in winter (December to February), 6 m s^{-1} in spring (March to May), 5 m s^{-1} in summer (June to August) and 8 m s^{-1} in autumn (September to November) (Vagenas et al., 2017). Thus, the periods for which we have noticed a maximum of oil detection, corresponds to periods when the wind is the weakest (Vagenas et al., 2017). At the same time, these wind values appear to be stable between the years (Soukissian and Sotiriou, 2022). The presence of a weaker wind period correlated with a higher detection rate suggest a meteorological control and best suitable detection conditions during the summer period.

4.1.2. Occurrence rate

The temporal distribution seems to be mainly influenced by wind conditions and shows that the summer periods are the most favourable for oil slick detection. The relative activity of seepage sites are usually compared using the ration between the number of detected slicks and number of available images (Oil slicks occurrence; Jatiault et al., 2017). Oil slick occurrence rates were calculated using the summer period data and analysis (Fig. 5) as it provides a more reliable estimation of the actual expulsion frequency.

Thus, the occurrence rate is higher than 5% for most active sites and are evenly distributed above this value, up to the maximum detected values of about 40%. The highest values are lower than the maximum occurrence rates detected in other active sites in the world (more than

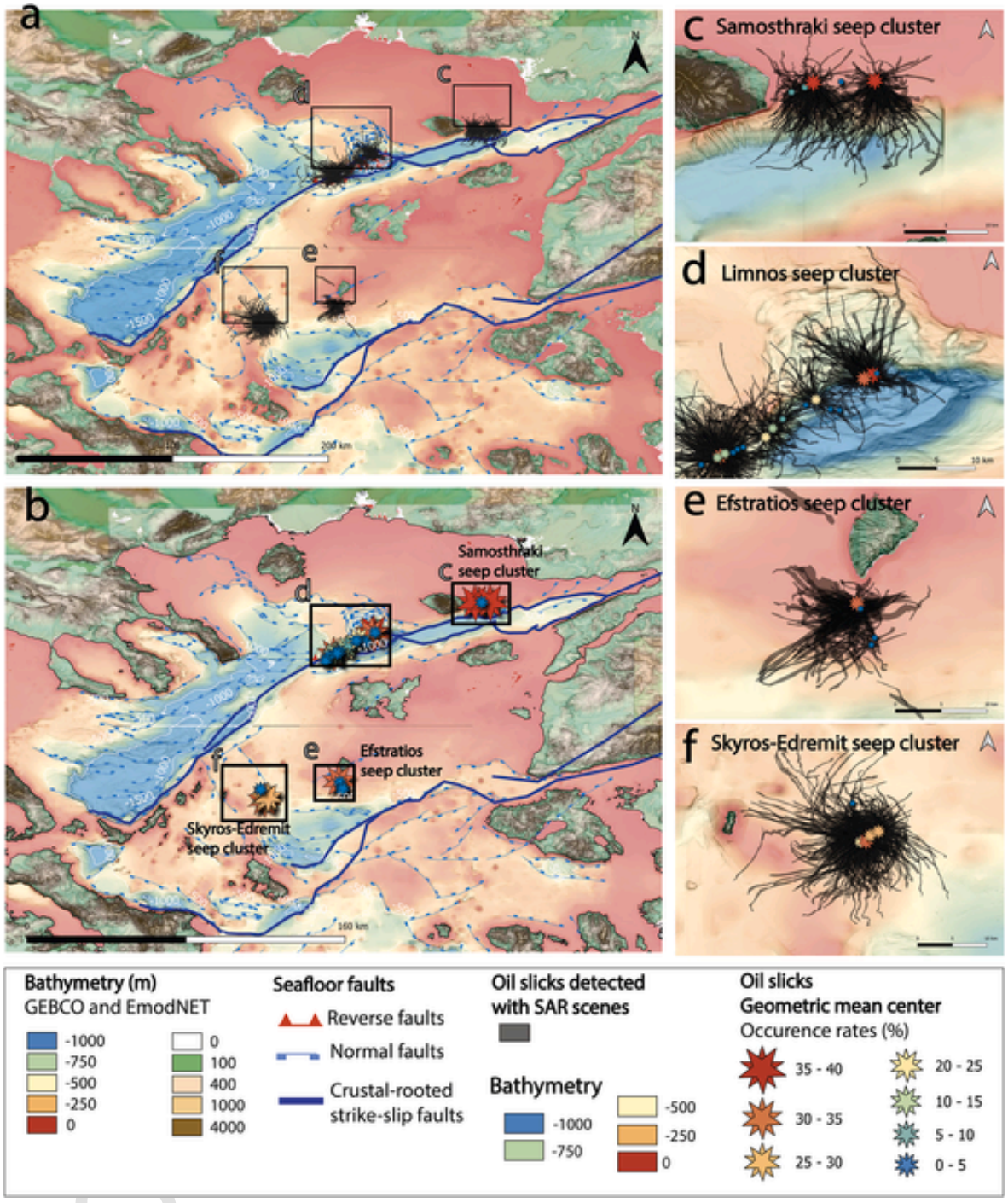

Fig. 3. a. Mapping results of detected recurrent oil slicks using repetitive SAR images. b, Heat map showing the oil slicks density and clusters. c, d, e, f: Zoom above of the four oil seeps clusters detected across the Aegean Sea.

75 % in the Gulf of Mexico and African margin; Garcia-Pineda et al., 2010; Jatiault et al., 2017). In agreement with other provinces, the Aegean oil seepage systems are therefore exclusively following a transient mechanism. The quiet periods are different from one seep to another and seem to be decorrelated even among oil seeps clusters (Fig. 3).

4.1.3. Water column and sea surface deflection

The geographical variability of the impact points (Fig. 6; Oil Slicks Origins-see left) compared to the mean centre (barycentre) enables an estimation of the vertical deflection distance distribution through the water column. The variability of the oil slicks location at the sea surface was calculated from the oil seep cluster of the Limnos basin, where the water depth of oil seeps at the seafloor ranges from 140 m up to 1200 m (Table 1). Except for the shallowest ones, the detected sites show average deflection values lower than the water depth (see Table 2).

For a water depth of 1000 m, the maximum observed deflection is 1700 m, with an average value around 300 m (Fig. 6). Most of the deflection is concentrated around values between 200 and 700 m. From the high variability in the orientation of the oil slicks, it appears that the combination of surface winds and surface currents are highly variable. There is no apparent main direction, the oil slicks are oriented homoge-

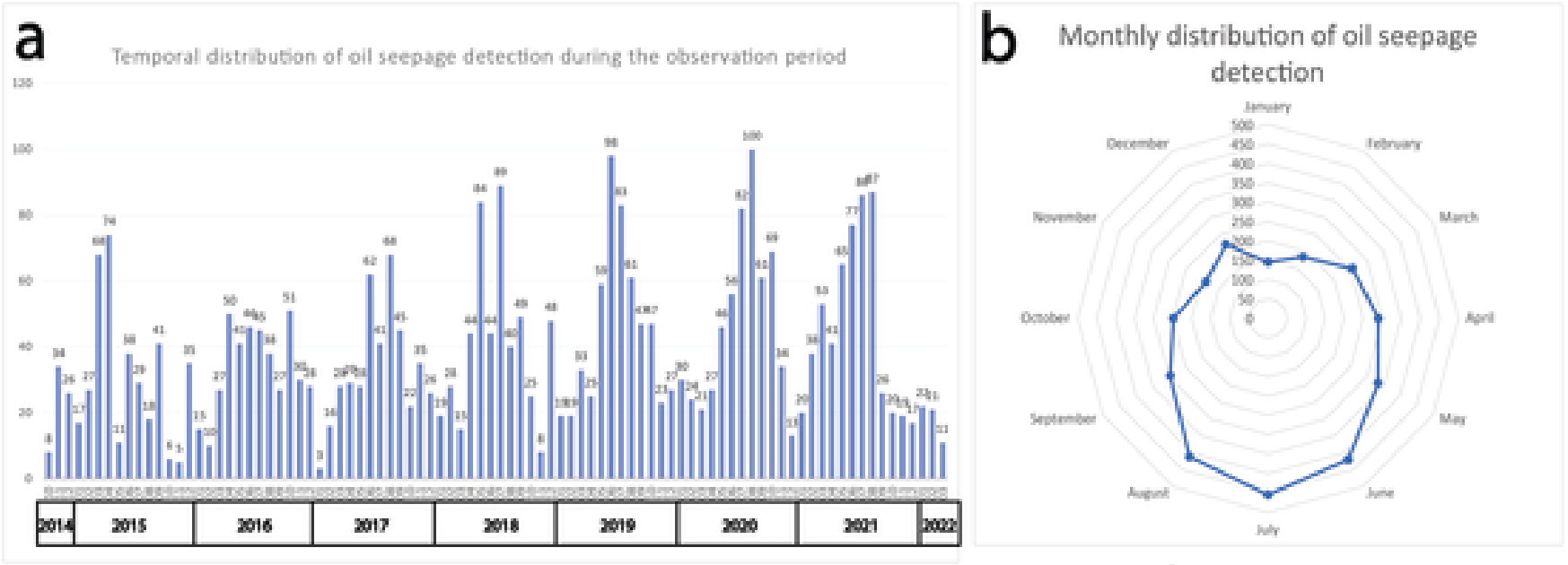

Fig. 4. a. Temporal distribution of slicks detection between October 2014 to March 2022. B. Radar graph showing the monthly distribution of oil slicks detection independently of the detection year.

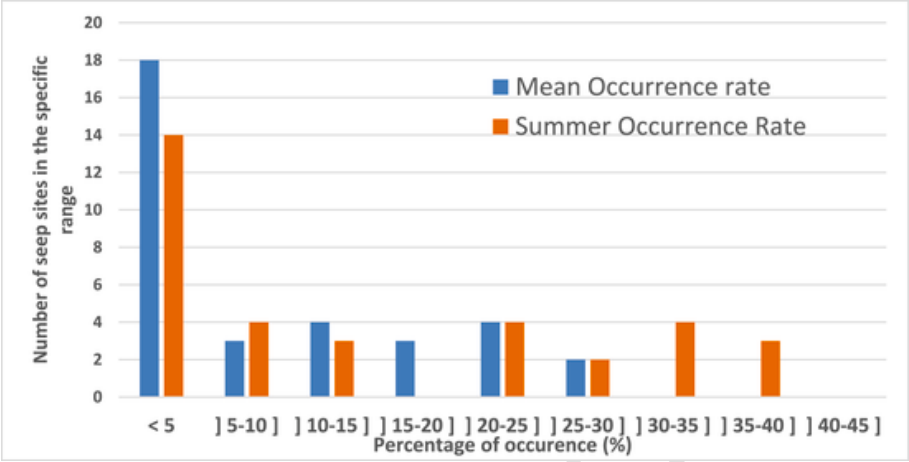

Fig. 5. Occurrence rate distribution for the entire data set (blue) and restricted to the analysis of images acquired during the summer period (Orange).

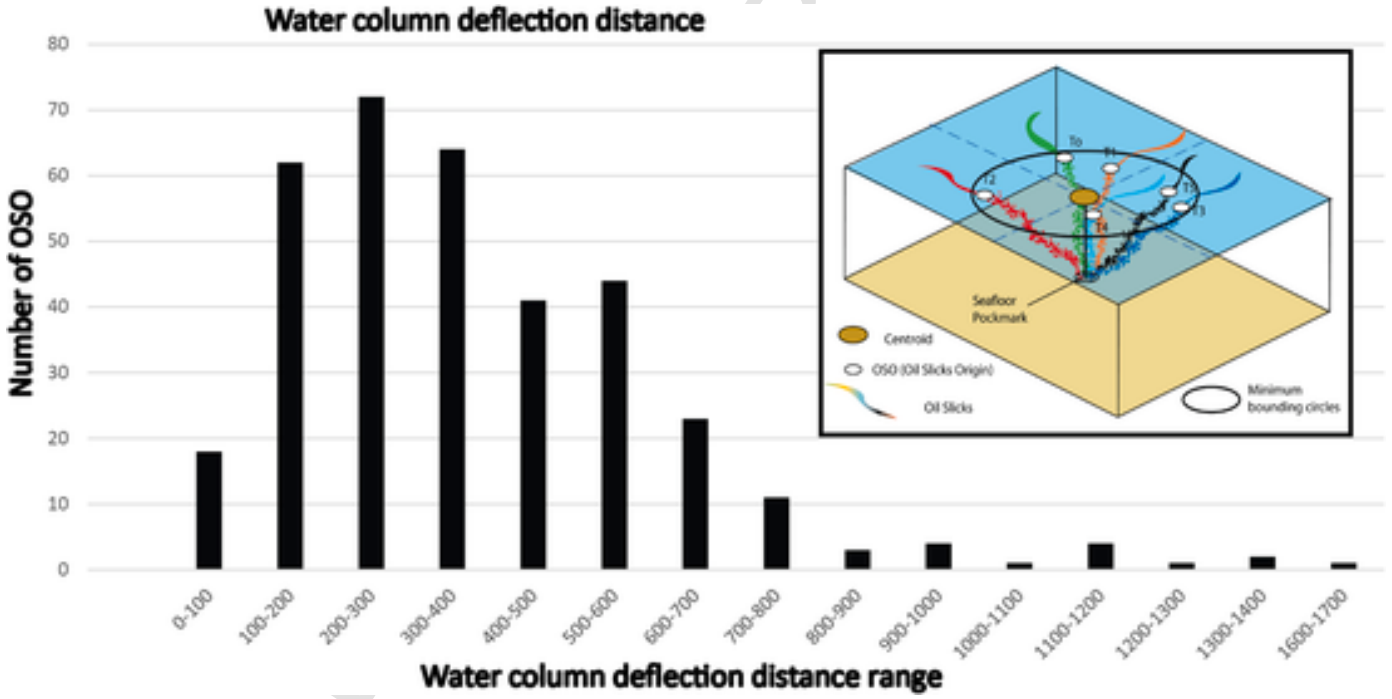

Fig. 6. Deflection distance distribution between the average impact point and OSO detected from spatial imagery. This graph indicates the spatial variability and impact area of oil slicks at the sea surface for 12 recurrent oil seeps of the Limnos basin.

neously from the central emission point (Fig. 3). The comparison between the average deflection distribution and the water depth (Table 1) suggest that most of the time, the deflection remains below the water depth values. The results rather agree with other published studies (Garcia-Pineda et al., 2010; Jatiault et al., 2018). The small location variability of the OSO observed at the sea surface suggest the deflection distance of oil droplet is low (Table 1) and therefore that the vertical projection of the oil seep sites on the bathymetry provides a good estimation of the seafloor vent location at the origin fluid expulsions.

4.2. The Limnos and saros basins

The Limnos basin corresponds to the most active oil seepage area among the Aegean Sea, with several seep sites detected (19) at the junction between the pull apart basin and the North Anatolian Fault (Fig. 7). The oil seepage detection is intermittent and occurred independently between oil seep sites and oil seeps clusters. Claw-shaped oil slicks (Fig. 7e, f, g, h) are typical of natural oil seepages and corresponds to concomitant expulsions of neighbour seep sites whose parallel patterns are induced by similar ocean conditions (winds and currents). These patterns detail multiple oil seepage sites among a seep cluster, where each identified claw corresponds to an individual seep site on the seafloor.

The Saros basin also show a concentration of 5 distinct oil seeps, at the east of Samothraki Island. This oil seep cluster is located on the continental shelf, at the edge of the Saros trough, with water depth values lower than 100 m (Fig. 3c).

In the Limnos trough, the presence of the Anatolian Fault seems to be a major element controlling the location of the detected expulsion sites (Fig. 8, Fig. 9). Indeed, all the detected sites are positioned along the main fault zone. This concentration leads to an alignment of natural expulsion sites. In the Limnos basin, oil seep sites are aligned along the N40° - N220° direction that corresponds quite well with the orientation of the NAF in the Limnos basin, as well as the reported location of the NAF in the Aegean Sea (Armijo et al., 1999; Şengör et al., 2005;

Table 1
Average deflection distribution calculated from several oil seep sites and compared to the water depth value. The values were computed for the oil seeps sites located among the Limnos basin. Ratio values above 1 suggest that the deflection is greater than the water depth in general, a ratio below 1 suggest that the deflection is most of the time lower than the water depth.

Oil seeps name	Average deflection (m)	Water depth (m)	Average deflection compared to the water depth
Efstr_4	188,63	139	1,35
NAF_1	376,68	565	0,66
NAF_2	304,13	562	0,54
NAF_3	291,63	580	0,50
NAF_6	279,90	410	0,68
NAF_7	172,75	580	0,29
NAF_8	6,19	462	0,01
NAF_9	385,52	525	0,73
SB_C_1	530,57	989	0,53
SB_C_2	84,07	1040	0,08
SB_C_3	47,57	1186	0,04
SB_E_1	429,45	310	1,38
SB_E_2	461,22	1010	0,45
SB_E_3	401,85	937	0,42
SB_W_1	465,21	434	1,07
SB_W_2	302,90	441	0,68
SB_W_3	271,01	574	0,47
Average values	**379,27**	**642**	**0,59**

Table 2
Oil flow rate estimated for each oil seep site.

Seep site	Estimated annual ouput (l/h)	Estimated annual ouput (m^3/year)	Seep site	Estimated annual ouput (l/h)	Estimated annual ouput (m^3/year)
Efstr_1	7,5	65,3	**SB_C_4**	0,1	0,9
Efstr_2	1,4	12,2	**SB_E_1**	6,3	55,4
Efstr_3	0,2	2,1	**SB_E_2**	5,7	49,6
Efstr_4	0,6	5,4	**SB_E_3**	0,2	2,1
Efstr_5	0,4	3,2	**SB_W_1**	3,1	26,8
NAF_1	7,0	60,9	**SB_W_2**	1,6	13,7
NAF_2	4,2	36,9	**SB_W_3**	1,1	9,8
NAF_3	2,3	20,0	**Sk-E_1**	1,1	9,5
NAF_4	0,3	2,9	**Sk-E_2**	1,8	15,5
NAF_5	0,3	2,6	**Sk-E_3**	0,9	8,3
NAF_6	0,2	1,5	**Sk-E_4**	0,0	0,2
NAF_7	0,2	1,8	**Sk-E_5**	1,2	10,7
NAF_8	0,2	1,3	**Smtk_1**	1,5	13,2
NAF_9	2,2	19,0	**Smtk_2**	0,4	3,5
SB_C_1	2,7	23,6	**Smtk_3**	0,3	2,5
SB_C_2	0,2	2,1	**Smtk_4**	1,9	16,5
SB_C_3	0,1	0,6	**Smtk_5**	0,0	0,4
			Total	**57,1**	**500,0**

Leptokaropoulos et al., 2012; Brun et al., 2016; Sakellariou et al., 2016).

The extensional component of the NAF becomes greater towards the West which results in the formation of multiple pull apart basins (Jolivet et al., 2008; Brun et al., 2016; Sakellariou et al., 2021). The Limnos and Saros basins are listed among the series of pull apart basins that developed in concomitance with the North Anatolian Fault (Fig. 3). The formation of these basins occurred in close relation with the propagation of the North Anatolian Fault toward the Aegean Sea, starting 3–5 Myr ago. A large translated sedimentary body is observed at the North of the Limnos basin. In the upslope domain, this slide is characterized by a series of arcuate concave escarpments interpreted as normal faults offsetting layered Quaternary deposits and by a downslope and distal convex toe associated with reverse faults ending in the Limnos pull-apart basin. This large-scale system probably roots on a deep listric fault, with greater depth than the penetration of the seismic profiles. Within this translated body, zones where the sedimentary layered structure appears disturbed or is not imaged may be interpreted as gravity-driven Mass Transport Deposits (MTD; Hampton et al., 1996; Moscardelli and Wood, 2008, 2016; Kneller et al., 2016; Nwoko et al., 2020), although some of the acoustic blanking may here also be a consequence of the presence of gas in the sediment. These MTD units appears buried beneath more recent sedimentary layers and thus probably represent past catastrophic events that affected parts of the moving slide. In addition, the steep slopes on either side of the basin display evidence of erosion by avalanches and/or currents as non-conformable sedimentary reflectors are interrupted near the seafloor. This multiple scale gravity-driven system in the northern part of the Limnos basin is presumably a consequence of the opening of the pull-apart basin, causing extensional stress around the releasing bend as well as a local steepening of the slopes. The scale of the slide is quite important (~20 km wide and >300 m thick; Fig. 9a and b), which suggests a buried weak layer locally present within the Tertiary series (Paleocene to Miocene) on the northern side of the NAF that has been activated as a decollement as the basin deepened. The internal deformation within this slide is moderate and it probably represents a continuous deformational system, although some parts of it may have been affected by catastrophic events. It is obviously still active considering that the seafloor fault scarps are visible on bathymetric maps and offsetting recent deposits (Fig. 8a).

The detected oil seeps sites are either located at the middle or at the basinward edge of the landslide, which suggest that oils (and probably other related fluid) were able to migrate through the MTDs probably through crustal deep-seated faults associated with the NAF. The natural expulsion zones (stars below) are located within a unique geological environment that combines strike-slip faulting (NAF) and gravity deformation associated with the formation of the pull-apart basin.

Based on the morpho-structural analysis of bathymetric features, active oil seeps clusters (boxes in the left) in the Limnos basin occur in various tectonic regimes.

- Cluster 1 (Fig. 8b) is located out of the pull-apart basin hosting the MTD, along a straight segment of the NAF, although quite close to its reported "turning point" (Sakellariou et al., 2016). Seeps are aligned on ridges parallel to the NAF 200–500 m south of the main fault trace. The tectonic regime is supposed to be prominently pure strike-slip.
- Cluster 2 (Fig. 8c) is located at the upper front of a compressional pop-up structure indicative of positive flower structure along the basin edge. This indicates a locally transpressive regime along the NAF. This pop-up structure is related to a restraining bend on the main fault between the pull apart basin and the straight segment where cluster 1 is located.
- Cluster 3 (Fig. 8d) is located close to the centre of the Limnos trough that corresponds to a pull-apart basin. Detected seepage sites locates at the exact location of the NAF at the seafloor which confirms that the NAF play a prominent role in the fluid migration from deep series. This cluster is also located in the central part of the former discussed MTD.

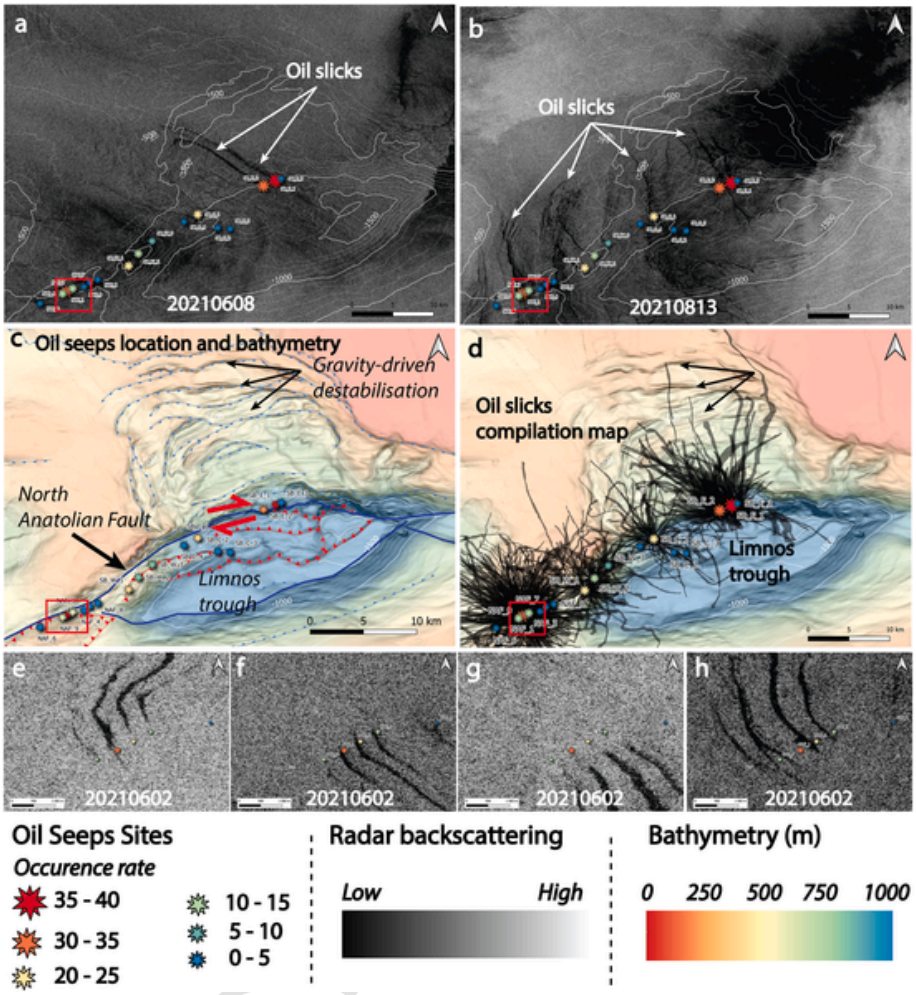

Fig. 7. a, b. Sea surface evidence of oil seepage detected with the satellite SAR system along the Limnos basins and nearby NAF. The shape and direction of oil slicks are induced by the sea surface currents and winds. Coloured stars show the centre of each recurrent seepage structure detected using the entire SAR data stack. The stars correspond to the best estimation of the active oil seeps sites on the seafloor. c Oil seeps location and d. Compilation map of the entire oil slicks mapping for the 2015–2022 SAR dataset along the Limnos basin and nearby NAF (location in Fig. 3d). e, f, g, h. Closer look of SAR images showing typical claw-shaped slicks at the eastern edge of the Limnos seep cluster (i.e., along the NAF). Each slick is associated with a distinct of seepage site.

The MTD show at least one offset zone induced by the NAF fault (Fig. 9). The NAF-induced offset depictable within the MTD implies that the sliding event occurred prior to the recent reactivation of the fault, at least regarding its distal part. This is consistent with a significant control of the NAF over the positioning of fluid expulsion systems, as it creates migration pathways crossing through the MTD up to the seafloor.

Between the Limnos basin and the Saros Gulf, oil seeps are only detected in two clusters East of Samothraki Island (Fig. 3c). The concentration of oil seeps at the East and centre part of the Limnos Trough (Figs. 7 and 8) therefore suggests an additional controlling factor of the oil seep emplacement. The absence of oil detection further East of the Limnos basin could be related to the absence of productive source rocks in this area. Onshore, the source rocks reported with a high oil potential correspond to the Late Eocene and Early Oligocene series of the Thrace basin, namely Hamitabat marine shales, Mezardere pro-deltaïc sediments and Danismen deltaic plain formations (Gürgey, 2009,2015; Siyako and Huvaz, 2007). Thrace basin formations are also the source of oil and thermogenic gas expelled at the Sea of Marmara seeps (Bourry et al., 2009; Ruffine et al., 2017, 2018). Oil seeps in the Sea of Marmara have been found on mud volcanoes located in the principal shear zone of the NAF and along splays bringing the productive Thrace basin formations to (or close to) the outcrop north of the deep basins (Sarıtaş et al., 2018; Grall et al., 2018). The most probable origin of the expelled oil is thus associated with a southern extension of the Thrace basin, even if its extension is not reported further south in the Aegean Sea. The Limnos Basin seeps are clearly associated with conduits in the NAF principal shear zone. The Samothraki seeps located on the shelf may be related to outcropping or sub-outcropping productive formations.

4.3. The Skyros-edremit trough

In addition, satellite images show the presence of highly active expulsion zones further south, in the vicinity of the Skyros-Edremit trough (Fig. 10). This area corresponds to a deformation zone between the NAF and the prolongation further West in the Aegean Sea to the southern branch of the North Anatolian Fault, namely the Skyros-Edremit fault. Although the margin structure knowledge is limited in this area, oil seeps appear surprisingly to be located at a distance of at least 10 km from the main reported deformation zones of the Skyros-Edremit fault corridor (Fig. 10; fault location depicted from seafloor morpho-bathymetric feature and Sakellariou et al., 2016; Brun et al., 2016; Erbil et al., 2021). Both oil seep clusters in the Skyros-Edremit region shows an alignment of the oil seeps, along the N60° (roughly parallel to Skyros-Edremit Fault) for the oil seeps located North of Skyros-Edremit and N155° for the oil seeps located south of Efstratios. The correspondence

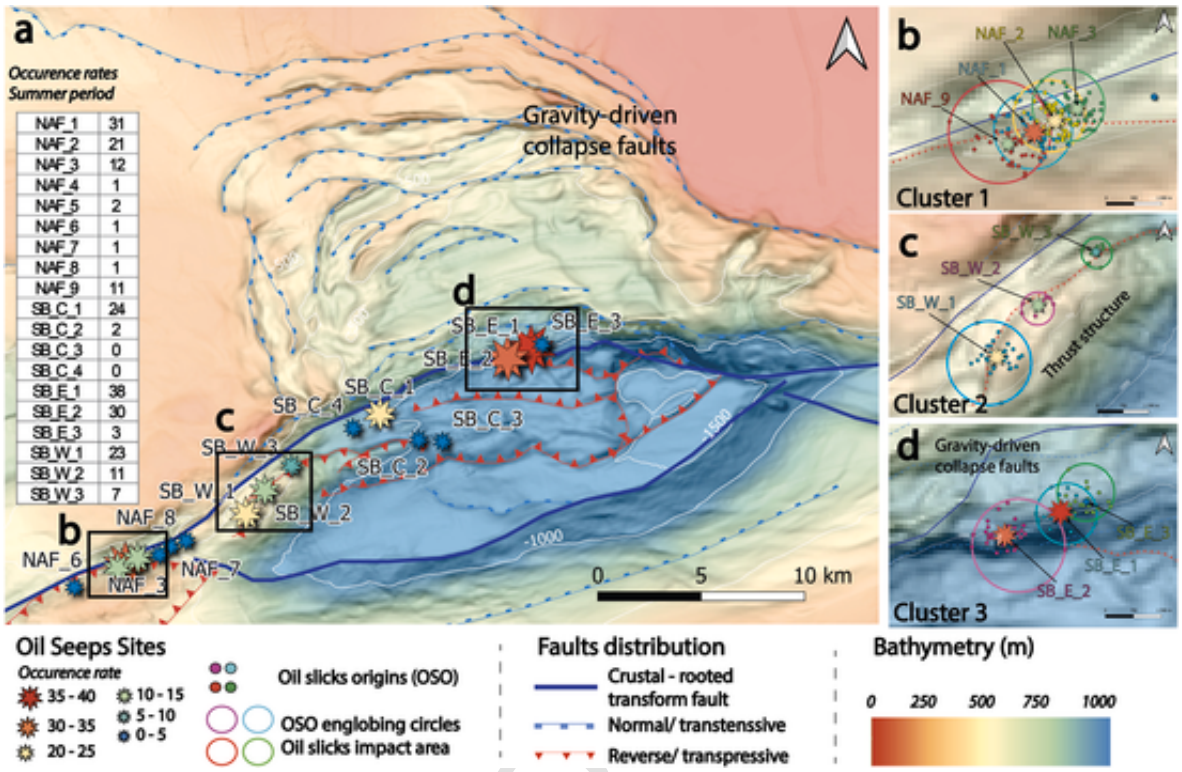

Fig. 8. Zoom on the Limnos basin and the detected oil seeps in this area. A. Local vision of the seep distribution correlated with the bathymetry and inferred locations of the faults, including the NAF and gravity-driven normal and reverse faults. Zoom above seep site clusters are displayed in b, c and d. Respectively along the strike slip NAF (b), over a transpressive area at the edge of the basin (c) and in the extensional centre of the basin (d).

in direction between the position of the oil expulsion sites among seep clusters and the direction of already identified faults is only valid for the cluster located south of Efstratios, which probably corresponds to the extensional fracturing system of the Skyros-Edremit trough (Horse tail system). The N60° orientation also suggest an underlying structural control for seepage location (Fig. 10d and e) but involves different fracturing direction in the area. The presence of intermediate, possibly deep, connections between the NAF and the SEF were reported in the area and with the same direction as the latter (Brun et al., 2016). Its end points towards the active cluster detected North-West of Skyros-Edremit and would have the same orientation as the alignment of the active sites identified using space imagery. By the way, focal mechanisms of earthquakes in this area as well as active faults on land in the Eubea region indicate some amount of distributed deformation, with dominant fault orientations NE-SW and NW-SE (Kassaras et al., 2020).

4.4. Reported seepage in the Aegean sea and along the North Anatolian Fault

Multiple cold seeps locations have been found across the Aegean Sea, notably along the Hellenic arc (Triantaphyllou et al., 2002; Megalovasilis, 2020). While gas compositions were analyzed, no oil fraction were previously reported. Moreover, these seeps are associated with the volcanic arc, a different geological context that in the study area, involving different seepage mechanisms. Alternatively, along the North Anatolian fault, the Sea of Marmara is a transform system that has been extensively explored for fluid seeps (Tryon et al., 2012; Dupre et al., 2015; Geli et al., 2018; Grall et al., 2018; Ruffine et al., 2018). Hydrocarbon seeps have been inventoried using geophysical data and water column imaging that primarily detect gas bubbles while the radar satellite-based detection method is only restricted to the liquid fraction. Oil seepages have been found in the Sea of Marmara by visual observations with manned submersibles and ROVs, but these findings are probably not exhaustive and may be complemented with radar satellite-based detection. On the other hand, the presence of a more distributed hydrocarbon seepage system involving gas is highly probable in the Aegean Sea, but its recognition would need further in situ investigation (Korber et al., 2014).

4.5. Possible origin of the expelled oil and fluid migration pathways

Hydrocarbon seepages are usually associated with fluid related bathymetric features such as mud volcanoes, mounds, or pockmarks (King and MacLean, 1970; Hovland, 1981; Hovland and Judd, 1988; Judd and Hovland, 2009; Hovland et al., 2010; Andresen and Huuse, 2011; Andresen, 2012). The size of pockmarks ranges from few meters (Hovland et al., 2010) up to the kilometre scale. Some of them can be isolated (Regab; Charlou et al., 2004; Ondreas et al., 2005; Gay et al., 2006; Marcon et al., 2014) or clustered (Jatiault et al., 2019a). The available bathymetry resolution (EMODNET binned 120 m) is probably too low to detect such features which explains the lack of detection of fluid-related seafloor features.

The availability of seismic sections in the Limnos basin (Fig. 9) allows a rough understanding of underlying structures and the general associated geological context, but remain too sparse to detect vertical successions of geophysical anomalies usually associated with the fluid ascent in the sediment series (vertical chimneys or pipes; Løseth et al., 2001, 2009, 2011; Cunningham and Lindholm, 2000; Heggland, 2002; Loncke and Mascle, 2004; Cartwright et al., 2007; Hustoft et al., 2009; Moss and Cartwright, 2010; Karstens and Berndt, 2015, Jatiault et al., 2019a, b). In the Sea of Marmara, the distribution of seeps results from concurrent updip migration along strata and upward migration along faults zones and fractures (Grall et al., 2018). Moreover, seeps related to main faults are found in a swath of about 1 km half-width along their trace at the seafloor, corresponding to a zone of diffuse deformation associated with the fault (Henry et al., 2018). North-East of Ganos, fluids

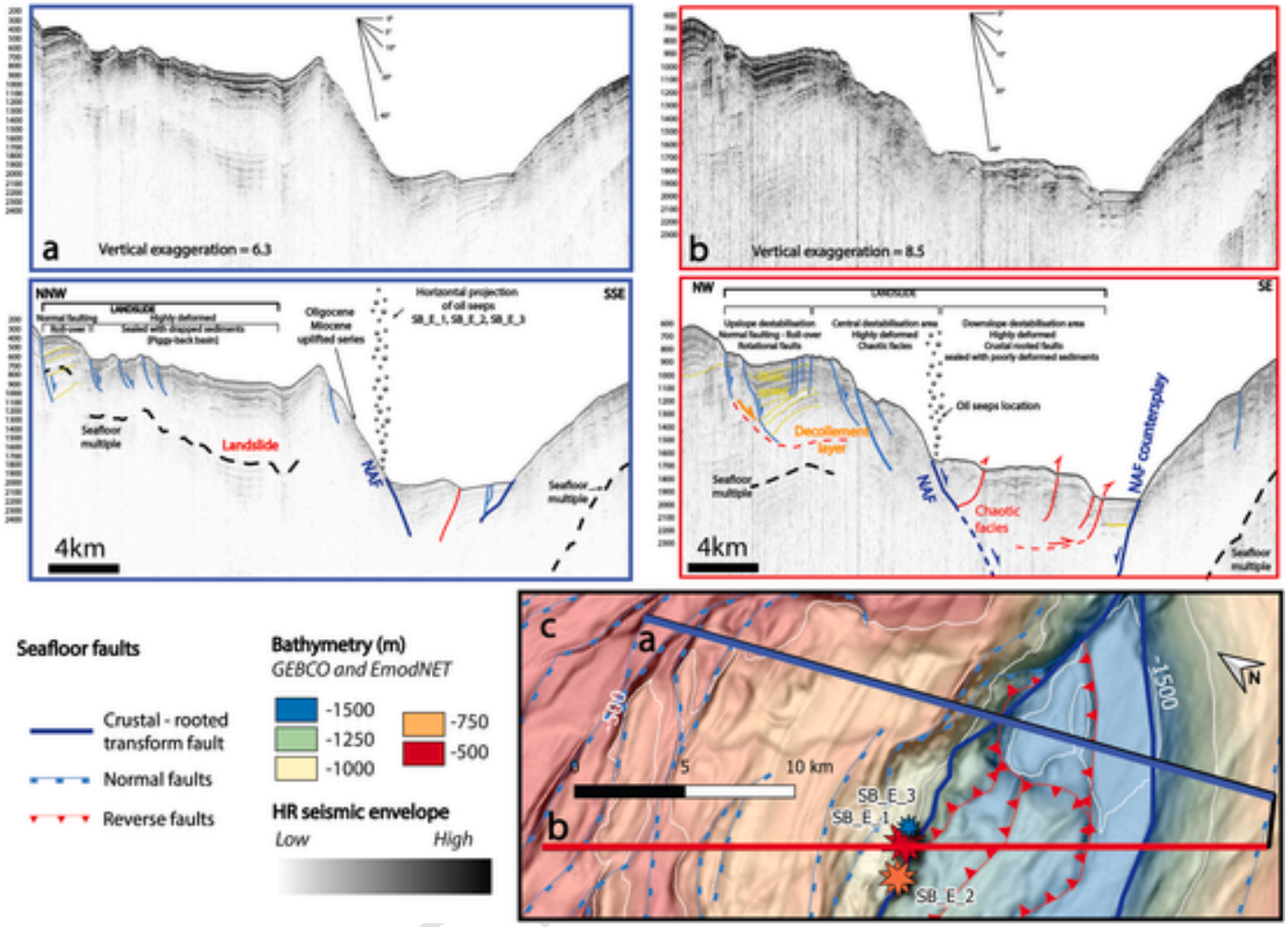

Fig. 9. a, b. Seismic profiles acquired across the Limnos basin located in the vicinity of active oil seep sites locations. Seismic sections are displayed using the envelope seismic attribute. c. Seismic section compared with oil seeps site locations.

are expelled from series at the base of Ganos scarp, which suggests that fluids migrate from below the basin and are focussed on the upper edge of the sediment fan (Grall et al., 2018). In this context, the conduits within the Thrace basin formation consist of extensional and transtensional structures. The distribution of oil seepages west of the Limnos trough on topographic highs close to the NAF may thus result from the same processes, fluids migrating upward in the fault zone at depth being collected on high points by the shallow sedimentary structure. The presence of seeps in the northern flank of the Limnos trough (Fig. 9c and d) may be also related to interaction between fault-related conduits at depth and shallow sedimentary structures. The most probable migration scenario considered for the Limnos Basin seeps would thus involve two stages.

The presence of hydrocarbon expulsions in both the northern area (North Anatolian Fault) and the southern domains (Skyros-Edremit Fault) raises the question whether these originate from a common source rock series. The only reported productive series in the area are the Upper Eocene-Oligocene shales of the Thrace basin (Siyako and Huvaz, 2007; Gürgey, 2009; 2015). The Thrace basin show a high oil potential in the onshore domain, Paleogene/Eocene silici-clastic source rocks (Elmas, 2012), however there is still no reported evidence of oil among the deep marine domain of the Aegean Sea. That would involve an extension of the Thrace productive series much further South of the NAF. Several gas fields are reported in the Northern part of the Aegean Sea, most of it being gathered among the continental shelves. Moreover, the oil seep sites of the Skyros-Edremit trough appear disconnected from the main SEF, which indicates a different seepage mechanism. A high hydrothermal activity is also reported across the Aegean Sea; even if most of the Aegean seep studies were concentrated along the Hellenic volcanic arc (Dando et al., 2000; Triantaphyllou et al., 2002; Megalovasilis, 2020), local hotspots (ascension of high temperature magmatic fluids) may also be considered as a potential source of heat that could trigger local thermal cracking of the organic matter.

The average bottom temperatures were measured in the Aegean oscillating between 10 and 18 °C (14 °C in average) in the Gulf of Thermaikos (Estournel et al., 2005; Sylaios, 2011), and were measured around 14 °C in deep basins (pers. comm. A. Karageorgis). Considering these temperatures, hydrate-bearing sediments are not expected for water depth shallower than 1100 m (Sloan and Koh, 2007; Camerlenghi et al., 2023) and slightly shallower for heavier hydrocarbon-bearing hydrates (structure II, H). Under these temperature and bathymetric conditions and assuming a 30 °C geothermal gradient, methane hydrates would only be stable of the deepest part of the Limnos basin and North Aegean trough with a maximum GHSZ thickness in the sediments of ~50 m below seafloor (calculated from hydrate stability profiles; Sloan and Koh, 2007). Even if hydrate may be found inside focused fluid pathways where thermogenic gasses are expelled (see mud volcanoes in the Sea of Marmara; Bourry et al., 2009; and in the Mediterranean Sea; De Lange and Brumsack, 1998; Merey and Longinos, 2018), the widespread hydrates presence is highly limited in the Aegean (Camerlenghi et al., 2023), which would explain the absence of a hydrate-related bot-

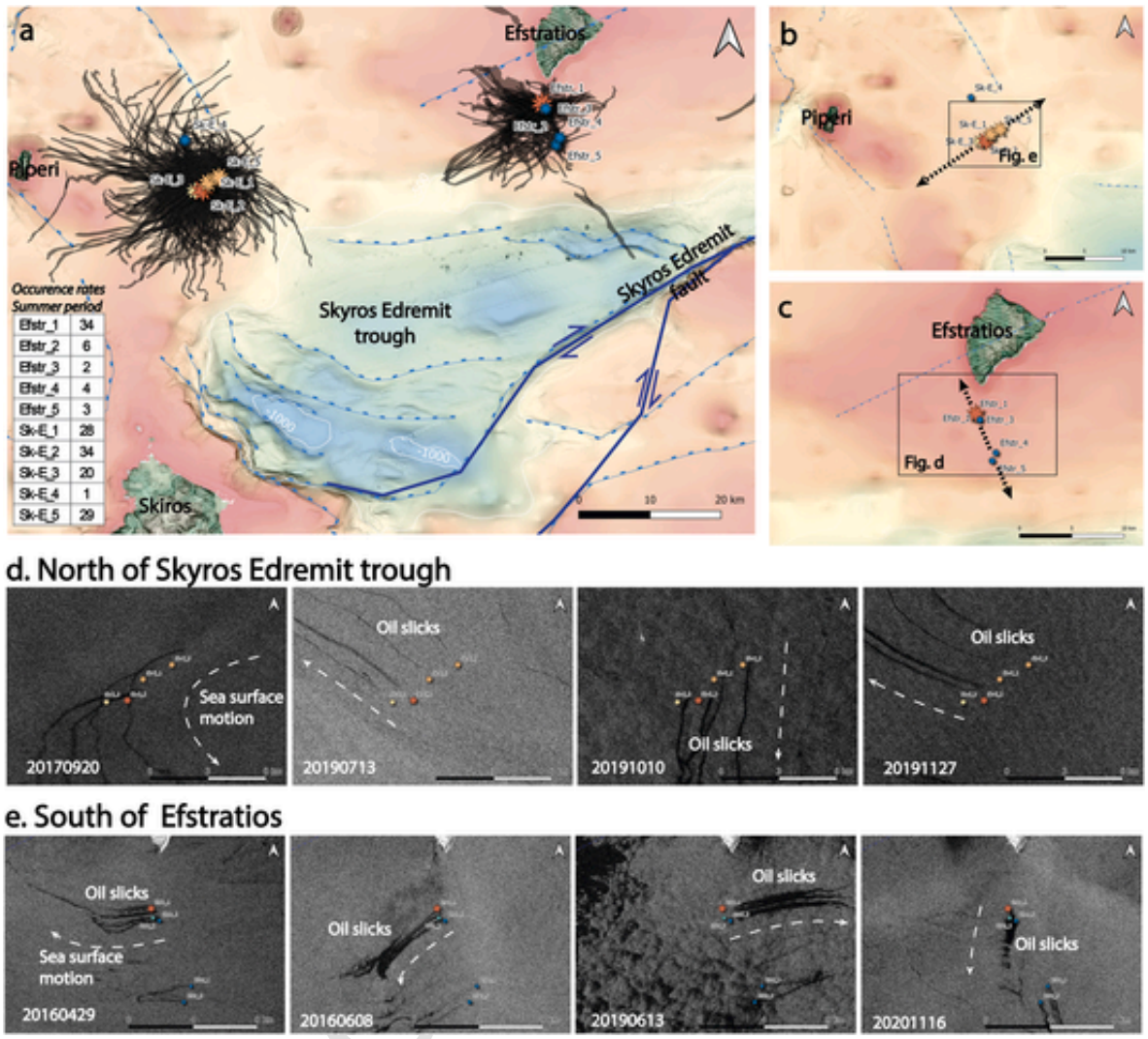

Fig. 10. Oil seepage detection in the Skyros-Edremit region. a. Compilation oil slicks map. B. Focus on the oil seep cluster located west of the Skyros-Edremit trough. C. Focus on the oil seep cluster located South of Efstratios.

tom simulating reflector (Shipley et al., 1979; MacKay et al., 1994; Berndt et al., 2005; Haacke et al., 2007).

4.6. Oil output estimation

Following the centerline method developed by Meurer et al., 2023), we dressed a first estimation of the expelled oil volume across the North Aegean Sea (Table 2). It is assumed that sea surface slicks are deflected by 3% of the sea surface wind and 100% of the sea surface currents (Kim et al., 2014). While a precise quantification would require the integration of both current velocity and orientation for both dataset and for each slick, a first idea of the expelled volumes can be computed assuming average surface velocity. The reported sea surface current at the oil seep sites ranges from 0 to 5 cm. s^{-1} for Samothraki basin, 15–25 cm s^{-1} for Limnos basin and 5–15 cm s^{-1} for Skyros-Edremit basin (Olson et al., 2007). The flow rate is calculated for each slick by considering this information, as well as attribute values such as the area and time of spreading (obtained with the centreline) and the thickness of the slick (estimated at 0.145 μm; Garcia-Pineda et al., 2014). The flow rate calculated for each oil slick was then used to calculate the average flow rate discharged by site over the entire observation period. This value is then normalised by the rate of occurrence calculated during the summer period (Figs. 7 and 10), considering the sites to be intermittent (Leifer et al., 2004; Greinert et al., 2006; Garcia-Pineda et al., 2010; Jatiault et al., 2017), thus making it possible to obtain flow rate values per site averaged over the observation period (Table 2). The flow rate calculated per site varies from 0.4 to 65 m^3 (0.4 and 7.5 l/h) per year, with an average value of 14.7 m3/year (1.7 l/h).

The volumes released per site are lower than those observed in other regions (Gulf of Mexico, in the Caspian Sea; or the Lower Congo basin; Jatiault et al., 2017) but can be explained by lower expulsion frequencies (38% maximum). The total volume expelled is estimated at 500 m^3 per year, the northern Aegean Sea ranks among the relatively active provinces, after the Gulf of Mexico (between 25 000 and 94 000 in the Gulf of Mexico; MacDonald et al., 2015), the Caspian Sea (1700 m^3; Zatyagalova et al., 2007) and the Lower Congo basin (4380 m^3; Jatiault et al., 2017). As similar studies, output estimations are substantially underestimated with the SAR technique because the thickness considered is the SAR lower detectability threshold.

5. Conclusion

The analysis of the Sentinel-1 dataset collection presented in this study reveals for the first time the presence of an active oil seepage system in the North Aegean Sea. Recurrent oil seepages were observed from 33 distinct emission sites that gathers among 4 seeps clusters. Oil seepages appear to be intermittent during the observation period and the seepage detection seems to be more effective during the summer

season. Considering the best detection conditions, the occurrence rate, computed from the ratio between the number of detected seepage and the useful dataset shows that occurrence rate values can reach 40 %. Active oil seeps sites occur in different tectonic domains. A first family of oil seeps are located along the North Anatolian fault along the Limnos and Saros pull apart basins induced by the transtensional stress regime along. A cluster has also been observed in the eastern edge of the Limnos basin in a more transpressional setting. For those active oil seeps, the NAF seems to have a prominent control regarding their location and dynamics. Another family of oil seeps is located further south in the Skyros-Edremit trough. The understanding of their emplacement is still enigmatic and requires further investigations to fully understand how the margin structure and deformation may control their location and dynamics. The total oil flow rate is estimate at 500 m^3 per year in the Aegean Sea.

CRediT authorship contribution statement

Romain Jatiault: Writing – review & editing, Writing – original draft, Visualization, Validation, Supervision, Software, Resources, Methodology, Investigation, Formal analysis, Data curation, Conceptualization. **Pierre Henry:** Writing – review & editing. **Lies Loncke:** Writing – review & editing. **Mahrez Sadaoui:** Writing – review & editing, Methodology. **Dimitris Sakellariou:** Writing – review & editing, Resources, Data curation.

Declaration of competing interest

The authors declare the following financial interests/personal relationships which may be considered as potential competing interests: Romain Jatiault reports administrative support provided by University of Perpignan Via Domitia. If there are other authors, they declare that they have no known competing financial interests or personal relationships that could have appeared to influence the work reported in this paper.

Data availability

Data will be made available on request.

References

Allen, A.A., Schlueter, R.S., Mikolaj, P.G., 1970. Natural oil seepage at coal oil point, santa barbara, California. Science 170, 974–977.

Andresen, K.J., 2012. Fluid flow features in hydrocarbon plumbing systems: what do they tell us about the basin evolution. Mar. Geol. 332–334, 89–108. https://doi.org/10.1016/j.margeo.2012.07.006.

Andresen, K.J., Huuse, M., 2011. 'Bulls-eye' and polygonal faulting in the Lower Congo Basin: relative timing and implications for fluid expulsion during shallow burial. Mar. Geol. 279, 111–127. https://doi.org/10.1016/j.margeo.2010.10.016.

Androulidakis, Y.S., Krestenitis, Y.N., Psarra, S., 2017. Coastal upwelling over the North Aegean sea: observations and simulations. Continent. Shelf Res. 149, 32–51.

Arango-Galván, C., Prol-Ledesma, R.M., Torres-Vera, M.A., 2015. Geothermal prospects in the Baja California peninsula. Geothermics 55, 39–57.

Armijo, R., Meyer, B., Hubert, A., Barka, A., 1999. Westward propagation of the North Anatolian fault into the northern aegean: timing and kinematics. Geology 27 (3), 267–270.

Barnes, P.M., Pondard, N., 2010. Derivation of direct on-fault submarine paleoearthquake records from high-resolution seismic profiles: wairu Fault, New Zealand. G-cubed. https://doi.org/10.1029/2010GC003254. . Q11013.

Bern, T.I., Wahl, T., Anderssen, T., Olsen, R., 1992. Oil Spill detection using satellite based SAR: experience from a field Experiment. In: Proceedings First ERS-1 Symposium - Space at the Service of Our Environment. pp. 829–834.

Berndt, C., Mienert, J., Vanneste, M., Bünz, S., 2005. Gas hydrate dissociation and sea-floor collapse in the wake of the Storegga Slide, Norway. In: Norwegian Petroleum Society Special Publications. Elsevier, pp. 285–292. (vol. 12.

Bohrmann, G., Heeschen, K., Jung, C., Weinrebe, W., Baranov, B., Cailleau, B., Heath, R., Hühnerbach, V., Hort, M., Masson, D., Trummer, I., 2002. Widespread fluid expulsion along the seafloor of the Costa Rica convergent margin. Terra. Nova 14 (2), 69–79. https://doi.org/10.1046/j.1365-3121.2002.00400.

Bourry, C., Chazallon, B., Charlou, J.L., Donval, J.P., Ruffine, L., Henry, P., et al., 2009. Free gas and gas hydrates from the Sea of Marmara, Turkey: chemical and structural characterization. Chem. Geol. 264 (1–4), 197–206.

Brekke, C., Solberg, A.H.S., 2005. Oil spill detection by satellite remote sensing. Rem. Sens. Environ. 95, 1–13. https://doi.org/10.1016/j.rse.2004.11.015.

Brun, J.P., Faccenna, C., Gueydan, F., Sokoutis, D., Philippon, M., Kydonakis, K., Gorini, C., 2016. The two-stage Aegean extension, from localized to distributed, a result of slab rollback acceleration. Can. J. Earth Sci. 53 (11), 1142–1157.

Canet, C., Prol-Ledesma, R.M., Dando, P.R., Vázquez-Figueroa, V., Shumilin, E., Birosta, E., et al., 2010. Discovery of massive seafloor gas seepage along the Wagner Fault, northern Gulf of California. Sediment. Geol. 228 (3–4), 292–303.

Camerlenghi, A., Corradin, C., Tinivella, U., Giustiniani, M., Bertoni, C., 2023. Subsurface heat and salts cause exceptionally limited methane hydrate stability in the Mediterranean Basin. Geology 51 (2), 162–166.

Camilli, R., Reddy, C.M., Yoerger, D.R., Van Mooy, B.A., Jakuba, M.V., Kinsey, J.C., et al., 2010. Tracking hydrocarbon plume transport and biodegradation at Deepwater Horizon. Science 330 (6001), 201–204.

Cartwright, J., Huuse, M., Aplin, A., 2007. Seal bypass systems. AAPG Bull. 91 (8), 1141–1166.

Charlou, J.L., Donval, J.P., Fouquet, Y., Ondreas, H., Knoery, J., Cochonat, P., Levaché, D., Poirier, Y., Jean-Baptiste, P., Fourré, E., Chazallon, B., 2004. Physical and chemical characterization of gas hydrates and associated methane plumes in the Congo–Angola. Basin Chemical Geology 205, 405–425. https://doi.org/10.1016/j.chemgeo.2003.12.033.

Crooke, E., Talukder, A., Ross, A., Trefry, C., Caruso, M., Carragher, P., Stalvies, C., Armand, S., 2015. Determination of sea-floor seepage locations in the Mississippi Canyon. Mar. Petrol. Geol. 59, 129–135. https://doi.org/10.1016/j.marpetgeo.2014.08.004.

Cunningham, R., Lindholm, R.M., 2000. AAPG Memoir 73, Chapter 8: Seismic Evidence for Widespread Gas Hydrate Formation. Offshore West Africa.

Dando, P.R., Aliani, S., Arab, H., Bianchi, C.N., Brehmer, M., Cocito, S., et al., 2000. Hydrothermal studies in the Aegean Sea. Phys. Chem. Earth - Part B Hydrol., Oceans Atmos. 25 (1), 1–8.

De Lange, G.J., Brumsack, H.J., 1998. The occurrence of gas hydrates in Eastern Mediterranean mud dome structures as indicated by pore-water composition. Geological Society, London, Special Publications 137 (1), 167–175.

de Lépinay, M.M., Loncke, L., Basile, C., Roest, W.R., Patriat, M., Maillard, A., De Clarens, P., 2016. Transform continental margins–Part 2: a worldwide review. Tectonophysics 693, 96–115.

Dong, Y., Liu, Y., Hu, C., MacDonald, I.R., Lu, Y., 2022. Chronic oiling in global oceans. Science 376 (6599), 1300–1304.

Dupre, S., Scalabrin, C., Grall, C., Augustin, J.M., Henry, P., Şengör, A.M., et al., 2015. Tectonic and sedimentary controls on widespread gas emissions in the Sea of Marmara: results from systematic, shipborne multibeam echo sounder water column imaging. J. Geophys. Res. Solid Earth 120 (5), 2891–2912.

Elmas, A., 2012. The Thrace Basin: stratigraphic and tectonic-palaeogeographic evolution of the Palaeogene formations of northwest Turkey. Int. Geol. Rev. 54 (12), 1419–1442.

Erbil, Ü., Okay, A.I., Hakyemez, A., 2021. Late oligocene—early Miocene shortening in the Thrace Basin, northern aegean. Int. J. Earth Sci. 110 (6), 1921–1936.

Espedal, H.A., Wahl, T., 1999. Satellite SAR oil spill detection using wind history information. Int. J. Rem. Sens. 20, 49–65.

Estournel, C., Marsaleix, P., Ulses, C., 2021. A new assessment of the circulation of atlantic and intermediate waters in the eastern mediterranean. Prog. Oceanogr. 198, 102673.

Estournel, C., Zervakis, V., Marsaleix, P., Papadopoulos, A., Auclair, F., Perivoliotis, L., Tragou, E., 2005. Dense water formation and cascading in the Gulf of Thermaikos (North Aegean), from observations and modelling. Continent. Shelf Res. 25 (19–20), 2366–2386.

Fingas, M., Brown, C., 2014. Review of oil spill remote sensing. Mar. Pollut. Bull. 83 (1), 9–23. https://doi.org/10.1016/j.marpolbul.2014.03.059.

Franceschetti, G., Iodice, A., Riccio, D., Ruello, G., Siviero, R., 2002. SAR raw signal simulation of oil slicks in ocean environments. IEEE Trans. Geosci. Rem. Sens. 40 (9).

Garcia-Pineda, O., MacDonald, I., Zimmer, B., Shedd, B., Roberts, H., 2010. Remote-sensing evaluation of geophysical anomaly sites in the outer continental slope, northern Gulf of Mexico. Deep-Sea research II 57, 1859–1869. https://doi.org/10.1016/j.dsr2.2010.05.005.

Garcia-Pineda, O., Zimmer, B., Howard, M., Pichel, P., Li, X., MacDonald, I.R., 2009. Using SAR images to delineate ocean oil slicks with a texture-classifying neural network algorithm (TCNNA). Can. J. Rem. Sens. 35, 411–421.

Garcia-Pineda, O., MacDonald, I., Shedd, W., 2014. Analysis of oil-volume fluxes of hydrocarbon-seep formations on the Green Canyon and Mississippi Canyon: a study with 3D-seismic attributes in Combination with satellite and acoustic data. SPE Reservoir Eval. Eng. 17 (4), 430–435.

Gay, A., Lopez, M., Cochonat, P., Levaché, D., Sermondadaz, G., Seranne, M., 2006. Evidences of early to late fluid migration from an upper Miocene turbiditic cannel revealed by 3D seismic coupled to geochemical sampling within seafloor pockmarks, Lower Congo Basin. Mar. Petrol. Geol. 23, 387–399. https://doi.org/10.1016/j.marpetgeo.2006.02.004.

Geli, L., Henry, P., Grall, C., Tary, J.B., Lomax, A., Batsi, E., et al., 2018. Gas and seismicity within the Istanbul seismic gap. Sci. Rep. 8 (1), 6819.

Girard-Ardhuin, F., Mercier, G., Collard, F., Garello, R., 2005. Operational oil-slick characterization by SAR imagery and synergistic data. IEEE J. Ocean. Eng. 30 (3), 487–495.

Grall, C., Henry, P., Dupré, S., Géli, L., Scalabrin, C., Zitter, T.A., et al., 2018. Upward migration of gas in an active tectonic basin: an example from the sea of Marmara. Deep Sea Res. Part II Top. Stud. Oceanogr. 153, 17–35.

Greinert, J., Artemov, Y., Egorov, V., De Batist, M., McGinnis, D., 2006. 1300-m-high rising bubbles from mud volcanoes at 2080 m in the Black Sea: hydroacoustic characteristics and temporal variability. Earth Planet Sci. Lett. 244 (1–2), 1–15.

Gürgey, K., 2009. Geochemical overview and undiscovered gas resources generated from Hamitabat petroleum system in the Thrace Basin, Turkey. Mar. Petrol. Geol. 26 (7), 1240–1254.
Gürgey, K., 2015. Estimation of oil in-place resources in the lower Oligocene Mezardere shale, Thrace Basin, Turkey. J. Petrol. Sci. Eng. 133, 543–565.
Haacke, R.R., Westbrook, G.K., Hyndman, R.D., 2007. Gas hydrate, fluid flow and free gas: formation of the bottom-simulating reflector. Earth Planet Sci. Lett. 261 (3–4), 407–420.
Hampton, M.A., Lee, H.J., Locat, J., 1996. Submarine landslides. Rev. Geophys. 34 (1), 33–59.
Heggland, R., 2002. Seismic evidence of vertical fluid migration through faults: applications of chimney and fault detection. In: Proceedings from AAPG Hedburg Conference. Vancouver.
Henry, P., Grall, C., Kende, J., Viseur, S., Özeren, M.S., Şengör, A.M.C., Dupré, S., Scalabrin, C., Géli, L., 2018. A statistical approach to relationships between fluid emissions and faults: the Sea of Marmara case. Deep Sea Res. Part II Top. Stud. Oceanogr. https://doi.org/10.1016/j.dsr2.2018.05.010. . 2018.
Henry, P., Lallemant, S.J., Le Pichon, X., Lallemand, S.E., 1989. Fluid venting along Japanese trenches: tectonic context and thermal modeling. Tectonophysics 160 (1–4), 277–291. https://doi.org/10.1016/0040-1951(89)90396-X.
Hensen, C., Duarte, J.C., Vannucchi, P., Mazzini, A., Lever, M.A., Terrinha, P., et al., 2019. Marine transform faults and fracture zones: a joint perspective integrating seismicity, fluid flow and life. Front. Earth Sci. 7, 39.
Hovland, M., 1981. A Classification of Pockmark Related Features in the Norwegian Trench. IKU, Institutt for Kontinentalsokkelundersøkelser.
Hovland, M., 2002. On the self-sealing nature of marine seeps. Continent. Shelf Res. 22 (16), 2387–2394.
Hovland, M., Judd, A.G., 1988. Seabed Pockmarks and Seepages: Impact on Geology, Biology and the Marine Environment. Graham and Trotman, London, p. 293p.
Hovland, M., Heggland, R., De Vries, M.H., Tjelta, T.I., 2010. Unit-pockmarks and their potential significance for predicting fluid flow. Mar. Petrol. Geol. 27, 1190–1199. https://doi.org/10.1016/j.marpetgeo.2010.02.005.
Hovland, M., Talbot, M.R., Qvale, H., Olaussen, S., Assberg, L., 1987. Methane-related carbonate cements in pockmarks of the North Sea. J. Sediment. Petrol. 57 (5), 881–892.
Hovland, M., Irwin, H., 1992. Habitat of methanogenic carbonate cemented sediments in the North sea. Bacterial Gas 157, 172.
Hustoft, S., Dugan, B., Mienert, J., 2009. Effects of rapid sedimentation on developing the Nyegga pockmark field: constraints from hydrological modeling and 3-D seismic data, offshore mid-Norway. G-cubed 10 (6).
Jatiault, R., Dhont, D., Besson, F., Tedetti, M., de Fommervault, O.P., Loncke, L., et al., 2021. Water column poly-aromatic hydrocarbon anomalies measured with submersible gliders in the Angolan natural oil seepage province. Deep Sea Res. Oceanogr. Res. Pap. 175, 103588.
Jatiault, R., Dhont, D., Loncke, L., Dubucq, D., 2017. Monitoring of natural oil seepage in the Lower Congo Basin using SAR observations. Rem. Sens. Environ. 191, 258–272. https://doi.org/10.1016/j.rse.2017.01.031.
Jatiault, R., Dhont, D., Loncke, L., de Madron, X.D., Dubucq, D., Channelliere, C., Bourrin, F., 2018. Deflection of natural oil droplets through the water column in deep-water environments: the case of the Lower Congo Basin. Deep Sea Res. Oceanogr. Res. Pap. 136, 44–61.
Jatiault, R., Loncke, L., Dhont, D., Dubucq, D., Imbert, P., 2019b. Geophysical characterisation of active thermogenic oil seeps in the salt province of the lower Congo basin. Part II: a regional validation. Mar. Petrol. Geol. 103, 773–791.
Jatiault, R., Loncke, L., Dhont, D., Imbert, P., Dubucq, D., 2019a. Geophysical characterisation of active thermogenic oil seeps in the salt province of the lower Congo basin part I: detailed study of one oil-seeping site. Mar. Petrol. Geol. 103, 753–772.
Johannessen, O.M., Sandven, M., Jenkins, A.D., Durand, D., Petterson, L.H., Espedal, H., Evensen, G., Hamre, T., 2000. Satellite earth observation in operational oceanography. Coast Eng. 41, 155–176.
Jolivet, L., Augier, R., Faccenna, C., Negro, F., Rimmele, G., Agard, P., et al., 2008. Subduction, convergence and the mode of backarc extension in the Mediterranean region. Bull. Soc. Geol. Fr. 179 (6), 525–550.
Jolivet, L., Faccenna, C., Huet, B., Labrousse, L., Le Pourhiet, L., Lacombe, O., et al., 2013. Aegean tectonics: strain localisation, slab tearing and trench retreat. Tectonophysics 597, 1–33.
Jollivet, D., Faugeres, J.C., Griboulard, R., Desbruyers, D., Blanc, G., 1990. Composition and spatial organization of a cold seep community on the South Barbados accretionary prism: tectonic, geochemical and sedimentary context. Prog. Oceanogr. 24 (1–4), 25–45.
Jones, D.O.B., Walls, A., Clare, M., Fiske, M.S., Weiland, R.J., O'Brien, R., Touzel, D.F., 2014. Asphalt mounds and associated biota on the Angolan margin. Deep-Sea Res. I. https://doi.org/10.1016/j.dsr.2014.08.010.
Joye, S.B., MacDonald, I.R., Leifer, I., Asper, V., 2011. Magnitude and oxidation potential of hydrocarbon gases released from the BP oil well blowout. Nat. Geosci. 4 (3), 160–164.
Judd, A., Hovland, M., 2009. Seabed Fluid Flow: the Impact on Geology, Biology and the Marine Environment. Cambridge University Press.
Karstens, J., Berndt, C., 2015. Seismic chimneys in the Southern Viking Graben–Implications for palaeo fluid migration and overpressure evolution. Earth Planet Sci. Lett. 412, 88–100.
Kassaras, I., Kapetanidis, V., Ganas, A., Tzanis, A., Kosma, C., Karakonstantis, A., et al., 2020. The new seismotectonic atlas of Greece (v1. 0) and its implementation. Geosciences 10 (11), 447.
Kim, T.H., Yang, C.S., Oh, J.H., Ouchi, K., 2014. Analysis of the Contribution of Wind drift factor to oil slick Movment under strong tidal condition. Hebei Spirit Oil Spill Case. Plos ONE 9 (1), e87393.
King, L.H., MacLean, B., 1970. Pockmark on the scotian shelf. Geol. Soc. Am. Bull. 81, 3141–3148.
Kneller, B., Dykstra, M., Fairweather, L., Milana, J.P., 2016. Mass-transport and slope accommodation: implications for turbidite sandstone reservoirs. AAPG Bull. 100 (2), 213–235.
Korber, J.H., Sahling, H., Pape, T., dos Santos Fereira, C., MacDonald, I., Bohrmann, G., 2014. Natural oil seepage at kobuleti ridge, eastern Black Sea. Mar. Petrol. Geol. 50, 68–82. https://doi.org/10.1016/j.marpetgeo.2013.11.007.
Le Pichon, X., Kreemer, C., 2010. The Miocene-to-present kinematic evolution of the Eastern Mediterranean and Middle East and its implications for dynamics. Annu. Rev. Earth Planet Sci. 38, 323–351.
Le Pichon, X., Chamot-Rooke, N., Rangin, C., Sengör, A.M.C., 2003. The North Anatolian fault in the sea of marmara. J. Geophys. Res. Solid Earth 108 (B4).
Le Pichon, X., Şengör, A.M.C., Kende, J., İmren, C., Henry, P., Grall, C., Karabulut, H., 2016. Propagation of a strike-slip plate boundary within an extensional environment: the westward propagation of the North Anatolian Fault. Can. J. Earth Sci. 53 (11), 1416–1439. https://doi.org/10.1139/cjes-2015-0129.
Leifer, I., Boles, J.R., Luyendyk, B.P., Clark, J.F., 2004. Transient discharges from marine hydrocarbon seeps: spatial and temporal variability. Environ. Geol. 46, 1038–1052.
Leptokaropoulos, K.M., Papadimitriou, E.E., Orlecka-Sikora, B., Karakostas, V.G., 2012. Seismicity rate changes in association with the evolution of the stress field in northern Aegean Sea, Greece. Geophys. J. Int. 188 (3), 1322–1338.
Loncke, L., Mascle, J., 2004. Mud volcanoes, gas chimneys, pockmarks and mounds in the Nile deep-sea fan (Eastern Mediterranean): geophysical evidences. Mar. Petrol. Geol. 21, 669–689. https://doi.org/10.1016/j.marpetgeo.2004.02.004.
Løseth, H., Gading, M., Wensaas, L., 2009. Hydrocarbon leakage interpreted on seismic data. Mar. Petrol. Geol. 26 (7), 1304–1319.
Loseth, H., Wensaas, L., Arntsen, B., Hanken, N., Basire, C., Graue, K., 2001,. 1000 m long gas blow-out pipes. In: 63rd EAGE Conference & Exhibition.
MacDonald, I.R., Guinasso, N.L., Ackleson, S.G., Amos, J.F., Duckworth, R., Sassen, R., 1993. Natural oil slicks in the gulf of Mexico visible from space. J. Geophys. Res. 98, 16351–16364.
MacDonald, I.R., Garcia-Pineda, O., Beet, A., Daneshgar Asl, S., Feng, L., Graettinger, G., et al., 2015. Natural and unnatural oil slicks in the G ulf of M exico. J. Geophys. Res.: Oceans 120 (12), 8364–8380.
Macgregor, D.S., 1993. Relationships between seepage, tectonics and subsurface petroleum reserves. Mar. Petrol. Geol. 10 (6), 606–619.
MacKay, M.E., Jarrard, R.D., Westbrook, G.K., Hyndman, R.D., 1994. Origin of bottom-simulating reflectors: geophysical evidence from the Cascadia accretionary prism. Geology 22 (5), 459–462.
Marcon, Y., Ondréas, H., Sahling, H., Bohrmann, G., Olu, K., 2014. Fluid flod regimes and growth of a giant pockmark. Geology 42 (1), 63–66. https://doi.org/10.1130/G34801.1.
Mascle, J., Martin, L., 1990. Shallow structure and recent evolution of the Aegean Sea: a synthesis based on continuous reflection profiles. Mar. Geol. 94 (4), 271–299.
McCandless, S.W., Jackson, C.R., 2003. Principles of Synthetic Aperture Radar in Synthetic Aperture Radar Marine User's Manual. pp. 1–24.
Megalovasilis, P., 2020. Hydrothermal fluid particle geochemistry of submarine vents in kos island, Aegean Sea East Mediterranean. Geochem. Int. 58, 574–597.
Merey, Ş., Longinos, S.N., 2018. Numerical simulations of gas production from class 1 hydrate and class 3 hydrate in the nile delta of the Mediterranean Sea. J. Nat. Gas Sci. Eng. 52, 248–266.
Meurer, W.P., Asl, S.D., O'Reilly, C., Silva, M., MacDonald, I.R., 2023. Quantitative estimates of oil-seepage rates from satellite imagery with implications for oil generation and migration rates. Remote Sens. Appl.: Society and Environment 30, 100932.
Moscardelli, L., Wood, L., 2008. New classification system for mass transport complexes in offshore Trinidad. Basin Res. 20 (1), 73–98.
Moscardelli, L., Wood, L., 2016. Morphometry of mass-transport deposits as a predictive tool. Bulletin 128 (1–2), 47–80.
Moss, J.L., Cartwright, J., 2010. 3D seismic expression of km scale fluid escape pipes from offshore Namibia. Basin Res. 22 (4), 481–501.
Najoui, Z., Amoussou, N., Riazanoff, S., Aurel, G., Frappart, F., 2022. Oil slicks in the gulf of Guinea–10 years of envisat advanced synthetic aperture radar observations. Earth Syst. Sci. Data 14 (10), 4569–4588.
Nwoko, J., Kane, I., Huuse, M., 2020. Mass transport deposit (MTD) relief as a control on post-MTD sedimentation: insights from the Taranaki Basin, offshore New Zealand. Mar. Petrol. Geol. 120, 104489.
Ondreas, H., Olu, K., Fouquet, Y., Charlou, J.L., Gay, A., Dennielou, B., Donval, J.P., Fifis, A., Nadalig, T., Cochonat, P., Cauquil, E., Bourillet, J.F., Le Moigne, M., Sibuet, M., 2005. ROV study of a giant pockmark on the Gabon continental margin. Geo Mar. Lett. 25, 281–292. https://doi.org/10.1007/s00367-005-0213-6.
Olson, D.B., Kourafalou, V.H., Johns, W.E., Samuels, G., Veneziani, M., 2007. Aegean surface circulation from a satellite-tracked drifter array. J. Phys. Oceanogr. 37 (7), 1898–1917.
Orange, D.L., Yun, J., Maher, N., Barry, J., Greene, G., 2002. Tracking California seafloor seeps with bathymetry, backscatter and ROVs. Continent. Shelf Res. 22 (16), 2273–2290.
Papanikolaou, D., Nomikou, P., Papanikolaou, I., Lampridou, D., Rousakis, G., Alexandri, M., 2019. Active tectonics and seismic hazard in Skyros basin, North Aegean sea, Greece. Mar. Geol. 407, 94–110.
Pierre, C., Fouquet, Y., 2007. Authigenic carbonates from methane seeps of the Congo deep-sea fan. Geo Mar. Lett. 27 (2–4), 249–257.
Reilinger, R., McClusky, S., Vernant, P., Lawrence, S., Ergintav, S., Cakmak, R., et al.,

2006. GPS constraints on continental deformation in the Africa-Arabia-Eurasia continental collision zone and implications for the dynamics of plate interactions. J. Geophys. Res. Solid Earth 111 (B5).
Römer, M., Sahling, H., Pape, T., Bahr, A., Feseker, T., Wintersteller, P., Bohrmann, G., 2012. Geological control and magnitude of methane ebullition from a high-flux seep area in the Black Sea—the Kerch seep area. Mar. Geol. 319, 57–74. https://doi.org/10.1016/j.margeo.2012.07.005.
Ruffine, L., Donval, J.P., Croguennec, C., Bignon, L., Birot, D., Battani, A., et al., 2017. Gas seepage along the edge of the Aquitaine shelf (France): origin and local fluxes. Geofluids 2017.
Ruffine, L., Donval, J.P., Croguennec, C., Burnard, P., Lu, H., Germain, Y., et al., 2018. Multiple gas reservoirs are responsible for the gas emissions along the Marmara fault network. Deep Sea Res. Part II Top. Stud. Oceanogr. 153, 48–60.
Sahling, H., Bohrmann, G., Spiess, V., Bialas, J., Breitzke, M., Ivaniov, I., Kasten, S., Krastel, S., Schneider, R., 2008. Pockmarks in the Northern Congo Fan area, SW Africa: complex seafloor features shaped by fluid flow. Mar. Geol. 249, 206–225. https://doi.org/10.1016/j.margeo.2007.11.010.
Sakellariou, D., Tsampouraki-Kraounaki, K., 2019. Plio-Quaternary extension and strike-slip tectonics in the Aegean. In: Transform Plate Boundaries and Fracture Zones. Elsevier, pp. 339–374.
Sakellariou, D., Rousakis, G., Drakopoulou, P., Tsampouraki-Kraounaki, K., Morfis, I., Panagiotopoulos, I., et al., 2021. Geomorphology, Geological Structure, Active Tectonics, and Basin Formation in the Aegean Sea.
Sakellariou, D., Rousakis, G., Vougioukalakis, G., Ioakim, C., Panagiotopoulos, I., Morfis, I., et al., 2016. Deformation pattern in the western North Aegean trough: preliminary results. Bull. Geol. Soc. Greece 50 (1), 124–133.
Sarıtaş, H., Çifçi, G., Géli, L., Thomas, Y., Marsset, B., Henry, P., et al., 2018. Gas occurrence and shallow conduit systems in the Western Sea of Marmara: a review and new acoustic evidence. Geo Mar. Lett. 38, 385–402.
Scardigli, A., Risser, L., Haddouche, C., Jatiault, R., 2023. Integrating unordered time frames in neural networks: application to the detection of natural oil slicks in satellite images. IEEE Trans. Geosci. Rem. Sens. 61, 1–14.
Schroot, B.M., Schüttenhelm, R.T., 2003. Shallow gas and gas seepage: expressions on seismic and other acoustic data from The Netherlands North Sea. J. Geochem. Explor. 78, 305–309.
Şengör, A.M.C., Tüysüz, O., Imren, C., Sakınç, M., Eyidoğan, H., Görür, N., et al., 2005. The North Anatolian fault: a new look. Annu. Rev. Earth Planet Sci. 33, 37–112.
Shipley, T.H., Houston, M.H., Buffler, R.T., Shaub, F.J., Mcmillen, K.J., Laod, J.W., Worzel, J.L., 1979. Seismic evidence for widespread possible gas hydrate horizons on continental slopes and rises. AAPG Bull. 63 (12), 2204–2213.
Sibuet, M., Juniper, K.S., Pautot, G., 1988. Cold-seep benthic communities in the Japan subduction zones: geological control of community development. J. Mar. Res. 46 (2), 333–348.
Siyako, M., Huvaz, O., 2007. Eocene stratigraphic evolution of the Thrace Basin, Turkey. Sediment. Geol. 198 (1–2), 75–91.
Skrunes, S., 2014. Characterization of low backscatter regions in the marine environment. In: Multipolarization C- and X- Band Synthetic Aperture Radar Data, Doctoral Thesis. The Arctic University of Norway, Tromsö, Norway.
Sloan, Jr, E.D., Koh, C.A., 2007. Clathrate Hydrates of Natural Gases. CRC press.
Solomon, E.A., Kastner, M., MacDonald, I.R., Leifer, I., 2009. Considerable methane fluxes to the atmosphere from hydrocarbon seeps in the Gulf of Mexico. Nat. Geosci. 2 (8), 561–565.
Soukissian, T., Sotiriou, M.A., 2022. Long-term variability of wind speed and direction in the mediterranean basin. Wind 2 (3), 513–534.
Spondylidis, S., Topouzelis, K., Kavroudakis, D., Vaitis, M., 2020. Mesoscale Ocean feature identification in the North Aegean sea with the use of sentinel-3 data. J. Mar. Sci. Eng. 8 (10), 740. https://doi.org/10.3390/jmse8100740.
Stock, J.M., Hodges, K.V., 1989. Pre-pliocene extension around the gulf of California and the transfer of baja California to the pacific plate. Tectonics 8 (1), 99–115.
Suess, E., 2014. Marine cold seeps and their manifestations: geological control, biogeochemical criteria and environmental conditions. Int. J. Earth Sci. 103, 1889–1916.
Sultan, N., Murphy, S., Riboulot, V., Géli, L., 2022. Creep-dilatancy development at a transform plate boundary. Nat. Commun. 13 (1), 1913.
Sylaios, G., 2011. Meteorological influences on the surface hydrographic patterns of the North Aegean Sea. Oceanologia 53 (1), 57–80.
Taymaz, T., Yilmaz, Y., Dilek, Y., 2007. The geodynamics of the Aegean and Anatolia: introduction. Geological Society, London, Special Publications 291 (1), 1–16.
Triantaphyllou, M.V., Baumann, K.H., Karatsolis, B.T., Dimiza, M.D., Psarra, S., Skampa, E., et al., 2018. Coccolithophore community response along a natural CO2 gradient off methana (SW saronikos gulf, Greece, NE mediterranean). PLoS One 13 (7), e0200012.
Triantaphyllou, M.V., Dermitzakis, M.D., Dimiza, M.D., 2002. Holo-and Heterococcolithophores (calcareous nannoplankton) in the gulf of Korthi (Andros island, Aegean Sea, Greece) during late summer 2001. Rev. Paleobiol. 21 (1), 353–369.
Tryon, M.D., Henry, P., Hilton, D.R., 2012. Quantifying submarine fluid seep activity along the North Anatolian Fault Zone in the Sea of marmara. Mar. Geol. 315, 15–28.
Tsampouraki-Kraounaki, K., Sakellariou, D., 2018. Seismic stratigraphy and geodynamic evolution of christiana basin, south aegean arc. Mar. Geol. 399, 135–147.
Tzali, M., Sofianos, S., Mantziafou, A., Skliris, N., 2010. Modelling the impact of Black Sea water inflow on the North Aegean Sea hydrodynamics. Ocean Dynam. 60, 585–596.
Vagenas, C., Anagnostopoulou, C., Tolika, K., 2017. Climatic study of the marine surface wind field over the Greek seas with the use of a high resolution RCM focusing on extreme winds. Climate 5 (2), 29.
Zatyagalova, V.V., Ivanov, A.Y., Gobulov, B.N., 2007. Application of Envisat SAR imagery for mapping and estimation of natural oil seeps in the South Caspian Sea. In: Proceedings of the Envisat Symposium 2007. pp. 23–27.
Zervakis, V., Krasakopoulou, E., Georgopoulos, D., Souvermezoglou, E., 2003. Vertical diffusion and oxygen consumption during stagnation periods in the deep North Aegean. *Deep Sea Research Part I*. Oceanographic Research Papers 50 (1), 53–71.
Zitter, T.A.C., Henry, P., Aloisi, G., Delaygue, G., Çagatay, M.N., Mercier de Lepinay, B., Al-Samir, M., Fornacciari, F., Tesmer, M., Pekdeger, A., Wallmann, K., Lericolais, G., 2008. Cold seeps along the main marmara fault in the Sea of marmara (Turkey). Deep-Sea Res. Part I Oceanogr. Res. Pap. 55, 552–570. https://doi.org/10.1016/j.dsr.2008.01.002.
Zitter, T.A., Huguen, C., ten Veen, J., Woodside, J.M., 2006. Tectonic control on mud volcanoes and fluid seeps in the Anaximander Mountains, eastern Mediterranean Sea. Geol. Soc. Am. Spec. Pap. 409, 615–631.